

---

Electrical Engineering Theses

Electrical Engineering

---

Spring 4-10-2023

## Automated Sensing Methods in Soft Stretchable Sensors for Soft Robotic Gripper

Prosenjit Kumar Ghosh

Follow this and additional works at: [https://scholarworks.uttyler.edu/ee\\_grad](https://scholarworks.uttyler.edu/ee_grad)



Part of the VLSI and Circuits, Embedded and Hardware Systems Commons

---

### Recommended Citation

Ghosh, Prosenjit Kumar, "Automated Sensing Methods in Soft Stretchable Sensors for Soft Robotic Gripper" (2023). *Electrical Engineering Theses*. Paper 56.

<http://hdl.handle.net/10950/4189>

This Thesis is brought to you for free and open access by the Electrical Engineering at Scholar Works at UT Tyler. It has been accepted for inclusion in Electrical Engineering Theses by an authorized administrator of Scholar Works at UT Tyler. For more information, please contact [tgullings@uttyler.edu](mailto:tgullings@uttyler.edu).

**AUTOMATED SENSING METHODS IN SOFT  
STRETCHABLE SENSORS FOR SOFT ROBOTIC GRIPPER**

by

Prosenjit Kumar Ghosh

A thesis submitted in partial fulfillment  
of the requirements for the degree of  
Master of Science in Electrical Engineering  
Department of Electrical and Computer Engineering

Prabha Sundaravadivel, Ph.D., Committee Chair  
College of Engineering

The University of Texas at Tyler  
May 2023

The University of Texas at Tyler  
Tyler, Texas

This is to certify that the master's thesis of

PROSENJIT KUMAR GHOSH

has been approved for the thesis requirements on  
April 10th, 2023.  
for the Master of Science in Electrical Engineering

Approvals:

DocuSigned by:



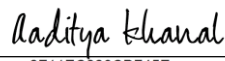
101C1CC8E9EC4E2...  
Thesis Chair: Dr. Prabha Sundaravadivel, Ph.D.

DocuSigned by:



0EE7E374D15143B...  
Member: Dr. Premananda Indic, Ph.D.

DocuSigned by:



2F11EC226CD745F...  
Member: Dr. Aaditya Khanal, Ph.D.

DocuSigned by:



7E4401EB0BCF49D...  
Chair: Dr. Hassan El-Kishky, Ph.D.

DocuSigned by:



3E50E32BE8F046A...  
Dr. Javier Kypuros, Ph.D.,  
Dean, College of Engineering.

## ACKNOWLEDGMENTS

I would like to express my sincerest thanks and appreciation to my thesis and graduate advisor, Dr. Prabha Sundaravadivel for her immense support and guidance. I am very appreciative of her patience, guidance, and encouragement that led to the successful completion of this thesis.

I would like to thank my thesis committee members, Dr. Premananda Indic and Dr. Aaditya Khanal for their support and counsel despite their busy schedules. To the Department of Electrical Engineering, I say a big Thank You for providing a conducive environment for making this thesis a success.

I would like to thank all my family, friends, colleagues in the lab, and entire students at the Department of Electrical Engineering for the encouragement and support that led to the success of this thesis.

# TABLE OF CONTENTS

## Contents

LIST OF TABLES .....	03
LIST OF FIGURES.....	04
Abstract .....	06
Chapter One INTRODUCTION.....	08
1.1 Aim/Objectives.....	10
1.2 Motivation .....	10
1.3 Organization of Thesis .....	11
Chapter Two LITERATURE SURVEY .....	12
2.1 Literature Survey of existing soft robotic actuators.....	12
2.2 Literature Survey of the existing soft sensor .....	14
Chapter Three TECHNICAL BACKGROUND.....	20
3.0 Modeling Actuator and Sensor.....	20
3.1 Actuator Design.....	21
3.1.2. Finite Element Method.....	22
3.1.3 Material Testing .....	23
3.1.4. FEM Software .....	23
3.1.5. Material Modeling.....	24
3.1.6. Meshing.....	24
3.1.6. Analysis Setting.....	24
3.1.6. Contacts.....	25
3.2 Soft Sensor Design.....	29
3.2.2. Design and Fabrication Methodology .....	29
3.2.2 Device Working Mechanism .....	32

Chapter Four METHODS AND FABRICATION PROCESS OF GRIPPER AND SENSOR.....	35
4.. Fabricated Gripper.....	35
4.1.1 Optimal Grasping Position .....	36
4.1.2. Data collection Control Unit for Gripper.....	39
4.2. Liquid Metal Preparation for Sensor .....	39
4.2.1. Liquid Metal Injection in Microchannel .....	43
4.2.1. Data Collection Unit for Sensor .....	46
Chapter Five DISCUSSION CONCLUSION AND FUTURE WORK.....	49
5.1. Output Characteristics of Gripper.....	49
5.2 Output Characteristics of Sensor .....	52
5.2.1. Stretchability.....	52
5.2.2. Gauge Factor .....	54
5.2.3. Linearity .....	55
5.2.4. Durability .....	56
5.3. Sensor Application .....	60
5.4. Machine Learning Model Proposition.....	61
5.4.1. Data Preprocessing .....	62
5.4.2. Classification Learning.....	63
5.5. Conclusion.....	73
References .....	74
Appendix .....	83

## LIST OF TABLES

Table 1: Comparison of popular actuation methods for soft robots .....	13
Table 2: Comparison between the different liquid metals alloy for sensor fabrication .....	15
Table 3: Fabrication printing methodology and application of the different flexible sensors. ....	17
Table 4: Geometric set-up of the soft pneumatic actuator .....	20
Table 5: Mechanical properties and hyperplastic model parameters. ....	22
Table 6: Integrated 3D printing of sensors. ....	34
Table 7: Thermal properties of Galinstan.....	40
Table 8: Collected data set and number.....	63
Table 9: Accuracy of the different classification models. ....	69
Table 10: Precision, Recall, and F1 Score of the Fine Tree Model.....	71
Table 11: Precision, Recall, and F1 Score of models Boosted Tree.....	72
Table 12: Precision, Recall, and F1 Score of the Bagged Tree.....	72
Table 13: Precision, Recall, and F1 Score of SVM Model.....	73

## LIST OF FIGURES

Figure 1: Schematic view of the pneumatic soft actuator.....	20
Figure 2: Schematic mechanism of the pneumatic soft actuator .....	21
Figure 3: Simple Neural Network .....	21
Figure 4: Flowchart of FEM simulation for Pneumatic soft robotic grip .....	25
Figure 5: FEM simulation for the soft pneumatic gripper (based on YEOH hyperplastic material model). The deformation result is at 30KPa.....	26
Figure 6: FEM simulation for the soft pneumatic gripper (based on YEOH hyperplastic material model). The deformation result is at 100KPa .....	27
Figure 7: Longitudinal cross-section under pressure.....	30
Figure 8: Cross-section view of the sensor.....	31
Figure 9: SLA printed soft robotic gripper.....	35
Figure 10: Optimal grasping position of Tape applied pressure 20KPa.....	36
Figure 11: Optimal grasping position of Tape dispenser applied pressure 20KPa.....	36
Figure 12: Optimal grasping position of Beaker applied pressure 50KPa.....	37
Figure 13: Optimal grasping position of Orange applied pressure 80KPa .....	37
Figure 14: Optimal grasping position of Ball applied pressure 100KPa .....	38
Figure 15: Control Unit Soft Robotic Gripper.....	40
Figure 16: Schematic view of flexible sensor.....	41
Figure 17: Schematic view of flexible sensor embedded with liquid metal .....	41
Figure 18: Schematic illustration of the sensor injecting Galinstan inside channel.....	42
Figure 19: The bottom lid of sensor (pre-mold processing) .....	42
Figure 20: Top lid of the sensor for the fabrication process .....	43
Figure 21: Fabrication process of soft sensor.....	43
Figure 22: The physical diagram of the preparation process of the liquid metal sensor.....	45
Figure 23: Schematic diagram of the preparation process (stretching condition).....	45



Figure 24: Schematic diagram after fabrication (bending condition) .....	46
Figure 25: Image of the fabricated stretchable sensor (thickness).....	46
Figure 26: A typical data acquisition process from the sensor.....	47
Figure 27: sensor response test by creating pressure.....	47
Figure 28: FEM vs Experimental result of bending angle with respect to applied pressure.....	49
Figure 29: FEM vs Experimental result of load test with respect to applied pressure.....	50
Figure 30: FEM vs Experimental result of elongation with respect to applied pressure. ....	51
Figure 31: Present the relationship between strain and resistance change.....	53
Figure 32: Shows the relationship between the gauge factor and strain.....	54
Figure 33: Represents the relative change of resistance with respect to applied pressure. ....	56
Figure 34: 1000 episodes of cyclic loading and unloading test at 30 kPa up to six minutes .....	57
Figure 35: 1000 episodes of cyclic loading and unloading test at 30 kPa (300 second period) .....	58
Figure 36: Performance test of the soft sensor using finger positioning.....	59
Figure 37: Output feedback of the sensor after creating pressure.....	60
Figure 38: Machine learning architecture.....	62
Figure 39: Methodology of the machine learning algorithm .....	62
Figure 40: The Standard error for height.....	63
Figure 41: The Standard error for weight.....	64
Figure 42: The Standard error for width.....	64
Figure 43: The confusion resistance changes .....	65
Figure 44: The confusion matrix .....	66
Figure 45: Confusion matrix for Fine tree model.....	67
Figure 46: Confusion matrix for ensemble boosted model.....	68
Figure 47: Confusion matrix for ensemble bagged tree model .....	69
Figure 48: Confusion matrix for SVM model .....	70

# **ABSTRACT**

## **Automated Sensing Methods in Soft Stretchable Sensors for Soft Robotic Gripper**

Prosenjit Kumar Ghosh

Thesis Chair: Prabha Sundaravadivel, Ph. D.

The University of Texas at Tyler

May 2023

A soft robot is made from deformable and flexible materials such as silicone, rubber, polymers, etc. Soft robotics is a rapidly evolving field where the human-robot-interaction and bio-inspired design align. The physical characteristics such as highly deformable material and dexterity make soft robots widely applicable. A soft robotic gripper is a robotic hand that acts like a human hand and grasps any object. The most common applications of soft robotics grippers are gripping and locomotion in sensitive applications where high dynamic and sensitivity are essential. Nowadays, soft robotics grippers are used without any sensing method and feedback as it is crucial to make the output feedback from the gripper. The major drawback of soft robotic grippers is their need for more precision sensing. In traditional robots, we can integrate any sensor to detect the force and orientation of objects. Still, soft robotic grippers rely on the deformation sensing method, where the sensor must be highly flexible and deformable. With a precise sensing method, it is easier to determine the exact position or orientation of the object being gripped, and it limits the application of the soft robotic gripper. Sometimes, soft robots are employed in harsh environments to solve problems. With the sensing feedback, automation may become more reliable and succeed altogether. So, in this research, we have designed and fabricated a soft sensor to integrate with the

gripper and to observe the feedback of the gripper. We propose integrated multimodal sensing that incorporates applied pressure and resistance change. The sensor provides feedback when the grippers hold any object, and the output response is the resistance change of the sensor.

The liquid metal is susceptible and can respond to low force levels. We presented the 3D design, FEM simulation, fabrication, and integration of the gripper and sensor, and by showing both simulation and experimental results, the gripper is validated for real-time application. FEM simulation simulates behavior, optimizing design and predicting performance. We have designed and fabricated a soft sensor that yields microfluidic channel arrays embedded with liquid metal Galinstan alloy and a soft robotic gripper hand. Different printing processes and characterization results are presented for the sensor and actuator. The fabrication process of the gripper and sensor is adequately described. The gripper output characteristics are tested for bending angle, load test, elongation, and object holding under various applied pressure.

Additionally, the sensor was tested for stretchability, linearity and durability, and human gesture integration with the finger, and this sensor can be easily reused/ reproduced. Furthermore, the sensor exhibits good sensitivity concerning different pressure and grasping various objects. Finally, we collected data using this sensor-integrated gripper and trained the dataset using machine learning models for automation. With more data, this can be an autonomous gripper with intelligent sensing methodologies. Moreover, this proposed stretchable sensor can be integrated into any existing gripper for innovative real-time applications.

# CHAPTER ONE

## INTRODUCTION

The innovation in the Internet of Things (IoT) system has reduced the gap between the real and the virtual world. Every day we are creating new kinds of hyper-connected societies where electrical devices are not only used for data collection and exchange but also for becoming more intelligent and context-aware. Furthermore, the advancement of multiple parameters such as sensing, data processing, cloud storage, and communication has made the system interact with the environment and developed the process via different learning algorithms using interactions. As a result, this help to create an intelligent space and self-protected design for health, mobility, digital society, food, energy, and environmental application.

The development of IoT process is developing from vertical to polymorphic applications. The system incorporated gadgets, sensors, programming, and devices are integrated for gathering and trading information to assume responsibility for things in the world. The IoT system is associated with the physical world, a hardware-based framework with outcomes of more productivity, precision, and benefit for the client. Moreover, a few challenges need to be addressed to provide a pervasive, unified, and seamless experience to the user. It is essential to make the system a standard of technology, interoperable module components supporting heterogeneous applications, low-cost IoT terminal, low power, reliable connection, and solutions guaranteeing end-to-end privacy and security. The Internet of Things (IoT) and Robotics are two separate fields. However, two different niches are growing simultaneously as every area is trying to align with the other. The IoT and the robotics communities are approaching to make a new term: Internet of Robotic things (IoRT). The main concept of IoRT is that all the intelligent devices can monitor the surroundings event, and the sensors can collect data, send the data to the server and the intelligence can decide upon the data. Consequently, they can manipulate or command the control of objects in the physical world. In the IoRT framework, the IoT network is connected to the internet including smart devices and IoT-enabled physical assets ranging from consumer devices to sensor-equipped connected technology. However, these parameters are important for customer-facing innovation, data-driven optimization, a new application, and digital transformation. IoT devices are designed and fabricated for particular types of tasks where the robotic system works as an assigned system. In this scenario, Artificial Intelligence (AI) and Machine Learning (ML) are used to help the robot to accomplish the job if any unexpected conditions arise. The IoT communities and robotics are

highly data-driven objectives. Considering the working perspective, the IoT communities have been involved with sensing, monitoring, and tracking where the robotic communities work for autonomous behavior, interaction with the environment, and production services. It is evident that two unique fields are merging to add values in a strong field. As a result, the concept of the “Internet of Robotic Things” aligns that gathering data from a wide range of sources, processed and transformed to a local server to control and manipulate to the physical world. For better task execution, it will be an excellent framework that the robot will get awareness from the IoT sensor and accomplish the job accordingly. Several aspects can be configured about IoRT: firstly, the robot can sense that it has embedded monitoring capabilities. Secondly, the IoRT can analyze information that’s mean there is edge computing involved. The main advantage of edge computing is that it can process data by itself and make decisions locally. Consequently, it doesn’t need to send data to the cloud for storage. Thirdly, the robot can get commands that it needs to execute. This collaboration is between machine to machine and between man to machine. The overall interactions can be considered as predictive maintenance and entirely new services

Sensing is the most vital part of IoT and wireless sensor networks. The data from the sensor are sent through the IoT network for post-analysis. The data from the sensor is valuable and the accuracy is important. There is an ISO standard that separates accuracy into precision and authenticity while emphasizing the integrity of a sensor. On the other hand, different sensing methods utilize the information from the sensing devices. However, the inherent EM nature uses different computing algorithms such as machine learning for classifying sensed information and presents additional challenges such as linearity, repetition resolution, hysteresis, stability, and calibration. However, it is more important to collaborate and develop energy-efficient routing protocols, optimization of communication links and adopt wake-sleep strategies. Data-driven strategies such as data reduction via controlling topology and incorporating renewable energy devices are very optimal for the IoT sensing framework. They are exploiting the wireless charging mechanism to solve the problem of the fundamental issue of power management. Especially for large heterogenous IoT networks, it is important to think about proper power management. Build an energy-constrained node with more functionality that compromises fidelity and power efficiency. New technologies and applications are surfacing every day and there still exist challenges and gaps to be addressed.

## **1.1 Aims:**

The motivation of this research is to develop a soft robotic gripper and flexible sensor that can be used for object identification. Sensitive flexible pressure sensors have numerous applications such as health monitoring, robotics, wearable system devices, rehabilitation, etc. As a result, we designed and fabricated an elastomer-based liquid metal flexible sensor, characterized the sensor, and observed the output. Moreover, we investigated a different application using our fabricated sensor. It is inevitable to use soft sensors to operate smoothly in soft robotic applications, and traditional sensors are incompatible with robotic applications as these types of sensors show large deformation. In this research, we have designed and fabricated a soft sensor that yields microfluidic channel arrays embedded with liquid metal Galinstan alloy. The fabricated soft sensor demonstrated excellent stability and reliability and exhibits promising sensitivity with respect to different pressure and conditions. Then the sensor is integrated with the soft robotic gripper to get sensing feedback. First, different fabrication steps such as 3D modeling, printing, fabrication and characterization result of the sensor and gripper. Then, sensorized gripper is used for data collection from different size and shape of objects. Finally, ML algorithm is used to validate the collected data.

## **1.2 Motivation:**

Internet-based health monitoring systems and wearable devices are increasing rapidly. Two important factors of precision health monitoring are accuracy and comfortable to the user. Flexible and wearable devices provide both possibilities to apply for plenty of applications. However, we tried to come up with a different application. As soft robotic applications are widely used to object detection and separation, a sensor integrated with the robotic hand will increase the efficiency of the robot. The pressure sensor shows excellent sensitivity with respect to object holding. Most of the current flexible and stretchable sensors are employed for health monitoring applications. In this paper, our main motivation is to design and fabricate soft sensor and robotic grippers. From the collected data, different machine-learning algorithms were applied to identify the object.

### **1.3 Organization of Thesis:**

The novel contribution of this research is to design and fabricate of the liquid metal-based flexible sensor, characterization of the sensor, and data collection. The research of this thesis is explained in five chapters: Chapter 2 describes the current research trend and literature review, Chapter 3 presents the design of the soft robotic gripper and sensor, Chapter 4 provides fabrication process of gripper and sensor, Chapter 5 describes the characterization, machine learning algorithm and conclusion.

# **CHAPTER TWO**

## **LITERATURE SURVEY**

### **2.1 Literature Review (Actuator):**

Soft robots are made of a soft and compliant material that can be continuously deformed and an infinite degree of freedom can be achieved. Physical characteristics of soft robots such as higher flexibility, safety, adaptable to harsh environments make them very popular in industries. Furthermore, the low impedance and passive deformation of the compliant material help to contact with various types of objects. However, the collaboration between humans and robots has gained substantial attention due to its very flexible handling and assembly.

There are plenty of applications for soft robotics due to their lightweight, easy-to-control, and cheap manufacturing cost. Mostly soft robotics are used in industries and healthcare applications. The broader applications are grasping [1], prosthetic hand [2], crawling [3], and so on. One of the great advantages of soft robotic is that it can handle any fragile object and objects with uneven shapes and sizes [4]. Soft actuators are the common type of soft robotic system and are mainly used in industries for versatile object handling. The most common type of actuator is soft pneumatic actuators [1]. The soft pneumatic actuators are very customizable, versatile mode of actuation and excellent compliance. Such kind of characterization of soft pneumatic actuators is to be considered for versatile application. The current models of soft pneumatic actuators are pneumatic network actuators [5], fiber reinforced actuators [6],[7] and McKibben actuators [8]. Pneumatic actuators (pneu-nets) are gaining popularity due to their physical properties such as customizability, softness, and ease of fabrication. The bending properties are also an important parameter to characterize their performance and application. However, material selection and printing technology need to be advanced to fabricate this actuator. Designing an actuator and getting perfect deformation behavior is the main goal of soft robotics and fiber-reinforced actuators can meet this design requirement.

However, conventional robots are restricted by degree of freedom (DoF) and the rigid body makes them very hard to manipulate for multiple tasks. As a result, these robots have limited dexterity and are not applicable in unstructured or very constrained workplaces [9] [10]. On the other hand,



soft robots are highly applicable where the environment is dynamic, sensitive to physical interactions or there is very restricted access [11] [12]. Most of the soft robots are bioinspired [13] and their design resembles nature or animals such as snakes [14] [15], worms [16] [17], fish [18] [19], and tentacles [20] [21].

There are multiple mechanisms have been used for the soft robotic control process. Gas or liquid is used to control the chamber inflation or deflation for the fluid-driven actuation [22]. And the cable-driven actuation process, pull and release cable which is embedded with the soft actuator are used to control the system [23] [24]. Moreover, temperature changes are also being applied for the shape memory materials (SMM) [25].

Actuation	Displacement	Fabrication	Control	Efficiency	Biocompatibility	Application
Pneumatic	Easy/High	High	Average	Average	Average	High
Hydraulic	Easy/High	High	High	Low	High	Average
Cable-Driven	Easy/High	High	Average	Average	Average	Average
EAP	Low	High	Average	High	Average	Low
SMM	Low	Average	High	Average	Average	Low
Electromagnetic	Average	High	High	High	High	Average
TCA	Average	Low	High	Average	Average	Low

Table 1: Comparison of popular actuation methods for soft robots.

For an electromagnetic-type soft robotic gripper, an electric potential is applied between the two electrodes of the soft dielectric [26]. Another type of actuator is the twisted and coiled actuator (TCA). For this actuator, motion is achieved by changing temperature for thermal expansion and shrink-like spring behavior [27]. In the field of soft robotics, the pneumatic actuator is the dominant method due to its lightweight, fabrication process, implementation, and efficiency [28]

[29]. Additionally, different kinds of soft materials can be used for the fabrication of soft pneumatic actuators such as diaphragm pumps or on/off solenoid valves. Compared to other types of soft actuators, soft pneumatic actuators are very high dexterity, safe, and have very large deformation. Both positive and negative pressure can be achieved from a soft pneumatic actuator. As a result, it is applicable where inversion pressure is vital for grasping. Also, negative pressure finds a fail-safe feature, improved lifetime, and durability. In contrast, vacuum pressure can be very efficient for constrained volume applications [30]. Also, the performance of a soft pneumatic actuator can be boosted using both negative and positive pressure [31]. Motion is one of the important parameters for soft pneumatic actuators. The efficiency of the actuator highly depends on the motion and bending structure. SPA demonstrates multiple types of motions strategy such as bending, extension, contraction, and twisting [32] [33]. Each type of motion can be applied to a variety of applications.

However, the fabrication process of SPA is divided into three main strategies: (i) modeling process, [34] (ii) 3-D printing using flexible filaments [35], and (iii) elastomeric resin [36]. As soft robotics is one of the emerging fields, there is a variety of way to fabricate it. Every research group fabricates its way to make the actuator less expensive, more durable, and higher efficient.

### **2.1.2: Literature Review (Sensor):**

Pressure and temperature measuring with the static and dynamic interactions between the contact surfaces have been a potential application for artificial skin, robotic arms, texture recognition to wearable computing. The advantages of the elastomer pressure sensor is that they are very soft, stretchable, and can be adjusted in a variety of methods. Elastomer-based capacitive and strain sensors by depositing carbon nanotubes on PDMS can detect at least 50KPa of pressure and accommodate strains up to 150% [34].

Material name	Electrical Conductivity ( $S.m^{-1}$ )	Thermal Conductivity ( $W.m^{-1}.K^{-1}$ )	Viscosity (Pa.s)	Surface Tension ( $N.m^{-1}$ )
Mercury [91]	$1.06 \times 10^6$	8.54	$1.5 \times 10^{-3}$	0.486
EGaIn [92]	$3.04 \times 10^6$	26.6	$1.9 \times 10^{-3}$	0.624
Galinstan [93]	$3.4 \times 10^6$	16.5	$2 \times 10^{-3}$	0.718

Table 02: Comparison between the different liquid metals alloy for sensor fabrication.

Another research group developed pressure sensors by embedding planar circuits that aligned with carbon nanotubes in a polyamide thin film [35]. There are many efforts using conductive textiles such as electrolytical and carbonic paint-treated cotton knit to make the conductive sensor. This kind of textile-based sensor can be used for safe human-machine interaction, and they are very convenient for stretchable applications.

Materials	Fabrication Methods	Performances			Applications
		Stretching	GFs	Linearity	
EGaIn-PDMS [36]	Printing technology	350%	1.6–3.2	Partly linear	Different health monitoring devices
AgNW-PDMS [37]	Micro-modeling Method	70%	2–14	Partly linear	Bending and motion detection

CNT-CB-PDMS [38]	Micromolding method	22.6%	29	Nonlinear	Health monitoring devices.
Graphene-PDMS [39]	Coating techniques	7.1%	2.4–14	Two linear regions	Wearable devices
GWFs-PDMS [40]	Coating techniques	30%	~106	Nonlinear	Health monitoring such as advanced therapies.
MWCNTs-PDMS [41]	Liquid phase mixing	45%	1.2	Nonlinear	Human motion and force detection.
AgNP-PDMS [42]	Printing technology	20%	4.7–12.5	Two linear regions	Human-machine interaction.
CNT-PDMS [43]	Printing technology	100%	$2 \times 10^4$	Nonlinear	Bending angle measurement.
GO-PDMS [44]	Filtration method	Bending radii (5cm–2.5cm)	–	Nonlinear	Interactive for human
Graphene nanocellulose-PDMS [45]	Filtration method	100%	7.1	Partly linear	Drug delivery measuring
Ti/Au-PDMS [46]	Micromolding method	-	–	Nonlinear	Artificial skin

GnPs-PDMS [47]	Micromolding method	<10%	27.7–164.5	Nonlinear	Human-machine interaction.
----------------	---------------------	------	------------	-----------	----------------------------

Table 3: Fabrication printing methodology and application of the different flexible sensors.

With the development of materials science and electronic technology, a variety of new conductive materials emerge in an endless stream, which provides the possibility to prepare functional biomedical electronic devices. There is plenty of application for soft electronic devices. Soft matter electronic devices have revolutionized the field of wearable computing, biomedical devices, and soft robotics application. Moreover, every field of application depends on good human-machine interactions that are safe and flexible with human tissue and motion. The sensor is very compatible with the human body because they do not contain any hard material and they are capable of complying with natural human tissue that can be used any support natural limb motion.

It is crucial to use soft sensors to operate smoothly in health monitoring and soft robotic applications, and traditional sensors are incompatible because they are comprised with electronic circuits and rigid materials. In-room temperature liquid metal-based sensor that is highly flexible and stretchable can be used. This type of liquid metal-based sensor can identify the elastic pressure and shear deformation. Soft matter electronic devices have revolutionized the field of wearable computing, biomedical devices, and soft robotics application. Moreover, every field of application depends on good human-machine interactions that are safe and flexible with human tissue and motion. Thin film elastomer has been widely focused on the field of soft matter engineering. Most of the elastomer sensors are embedded with liquid metal that exhibits a broad range of electronic and sensing functionalities. The sensor is very compatible with the human body because they do not contain any hard material and they can comply with natural human tissue that can be used any support natural limb motion. Elastomer-based electronics and sensing devices are very promising though they are still in very nascent stages of development. There are a few challenges such as logic functionality, integration with external hardware, and a proper scalable manufacturing process. Elastomer-based electronics and sensing devices are very promising though they are still in very nascent stages of development. There are a few challenges such as logic functionality, integration with external hardware, and a proper scalable manufacturing process.

Additionally, the availability of flexible and stretchable materials and novel fabrication method, deformable electrodes are very auspicious for a stretchable sensor for exciting applications. Flexible sensors have earned a substantial attraction in the field of robotics due to their physical properties. Flexible sensors are widely being used in soft robotics [48], e-skin [49], and consumer electronics [50]. In particular, soft robotics need a sensor that performs different kinds of tasks in an unstructured environment. Aimed at different kinds of problems diverse materials have been used to gain high sensitivity and stretchability. However, sensitivity and stretchability are highly dependent on the material's embedding, depositing, and printing process [51-52]. For microelectromechanical technology, soft materials such as Polydimethylsiloxane (PDMS), and Ecoflex 00-30 are mostly used the shore hardness is very low.

Flexible and stretchable sensors have gained substantial attention because of their characteristics, low modulus, and lightweight [53-54]. However, all of these sensors don't represent strains over 100% which is a restriction of large-scale fabrication. At the same time, there are other new features such as delamination and rigid electric material available in the flexible sensor. Durability is one of the important factors for the flexible sensor there are several tests have been conducted after fabrication and it is needed to make sure that the sensor is long-lasting enough for real-life application. The variety of Young's modulus is responsible for the poor durability between rigid conductors and soft materials. To remove the Young modulus mismatch, different kinds of materials have been explored. Liquid metal has gained attention due to its low Young's modulus and high durability that is maintained for large strains [55-56]. Moreover, researchers are aware of the physical properties of the liquid material that create stretchable conductors and promising candidates for high-performance stretchable sensors. It is mentionable that Wenlong Cheng fabricated a durable and long-term flexible sensor by using an ionic liquid which brought out the solution of mechanical-mismatch errors [58]. The researcher has invented several types of conductive liquid materials such as eutectic gallium-indium (EGaIn) and Galinstan [59-61]. Mercury is also another familiar liquid material, but they are toxic and harmful.

Traditionally designed sensors are very rigid, and their surface is not suitable for their body skin or robotic hand. All of these parameters reduce the efficiency and haptic sensing. As a result, it is very important to design and fabricate a tactile sensor with high flexibility and ductility [62-64]. Moreover, in recent years the design and manufacturing process has gained substantial progress in

the field of flexible tactile sensors. The main drawback of the tactile sensor is that it can be used only for one kind of sensing application, thus cannot be applicable for the multifunctional haptic feedback system. There is plenty of research going on about to perceive more comprehensive tactile sensing. A lot of researchers already proposed multifunctional tactile sensors with different materials for instance Wang et al. [65] introduced the direct writing of laser-induced graphene (LIG) on the textile. The potential application of this sensor is to detect the ECG signal and NO<sub>2</sub>.

Silk -nanofiber-based carbon fiber membranes can be used for temperature and sensor sensing [66]. Therefore, it is very significant to develop multifunctional tactile sensors. Different kinds of materials such as carbon material including carbon nanotubes [67-69] natural -biomaterial-derived carbon [70], silver nanoparticles [71] hydrogels [72 ] and liquid metal [73-74] have been widely used for the fabrication of the tactile sensor. The advantage of liquid metal is that it can be used at room temperature. Liquid metal demonstrates high electrical conductivity and deformability which turns to highly durable and stable for tactile sensing [75-76]. For sensors, the fabrication process is vital because a slight change of material can decrease drastically the performance of the sensor. For the liquid metal sensor, it is very important to select a suitable fabrication process. There are a few fabrication processes that are commonly used for liquid metal including mask deposition [78], injecting material into microchannel [79-80], and direct writing/printing [81] Most of the researchers used their own methods to fabricate the sensor such as stainless steel has been used for patterning [82] and a rolling brush was used to print on an Eco-flex substrate.

The developed sensor was designed and fabricated for wearable and wireless healthcare applications. Another research group developed a multimode printing process to fabricate flexible electronics [83-84]. This fabrication process maintains the extrusion printing of elastomer layers and sprays printing of liquid metal slurry. The modern design is like digital light processing (DLP) based printing has been used for the microfluidic channels for lab-on-chip [87-90]. However, DLP based printing process is not efficient at all and still needs to be improved.

# CHAPTER THREE

## Modeling of Actuator and Sensor

### 3.1 Actuator design:

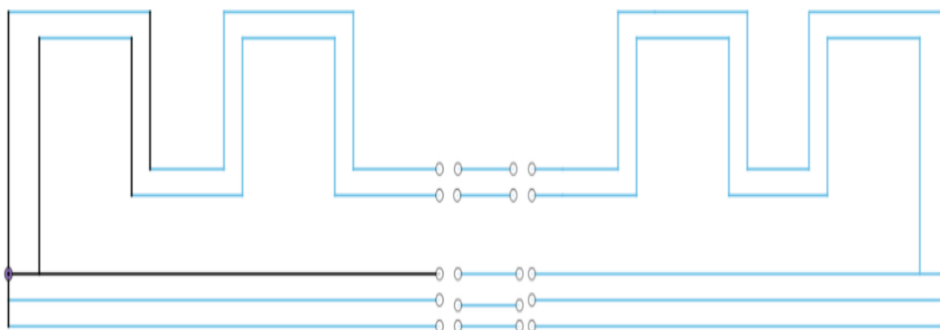


Figure 1: Schematic view of the pneumatic soft actuator. Size and dimension of each chamber.

Specimen Number	Width (w)	Wall thickness (w)	Height (h)	Gap (mm)	Channel Height (mm)
1	17.5	1.5	10	2.0	4
2	17.5	2.5	10	2.0	4
3	17.5	2.5	10	2.0	4
4	17.5	2.5	10	2.0	4

Table 4: Geometric set-up of the soft pneumatic actuator.



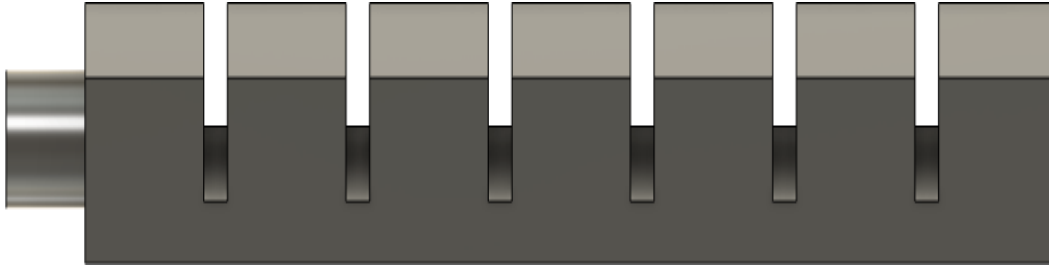


Figure 2: Schematic mechanism of the soft robotic gripper.

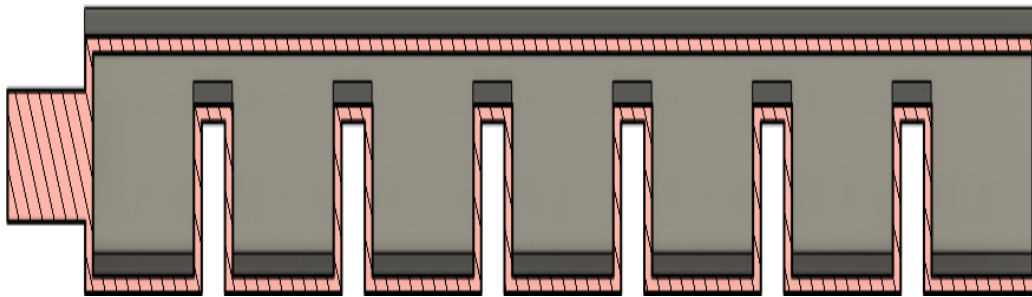


Figure 3: Cross-section view of the proposed soft robotic gripper.

The proposed SPA consists of a series of chambers and channels. The chambers are made of two layers: the top layer and the bottom layer. The top main body is an elastomer and the bottom is inextensible embedding an inextensible paper layer. The gripper is made of flexible material that lacks of any discrete connection. The bi-directional bending that applied under positive pressure and falls backward under negative vacuum pressure. The wall is designed with a fixed degree of the wedge so that it is favorable to increase the bending angle when it needs to bend backward. Moreover, the same design is used for the inner chamber and the thickness of the wall is constant when it increased the air pressure. This gripper is 112 mm long and 25 mm wide. The gripper is designed like that a flexible sensor can be adjusted in the bottom layer. The useful part of the gripper is 90 mm and rest of the portion is clamped with the stand with a fixator.

### 3.1.2 Finite Element Method:

Most of soft robots are fabricated of silicone rubbers and the actuation method is used by hydraulic or pneumatic actuation. The geometrics of soft actuators are very complex and nonlinear. As a result, it is very hard to develop an analytical model to describe their motion. One of the potential solutions is Finite Element Modeling (FEM) which provides an effective solution and can predict the performance and optimize the actuator design. From the literature review following conclusion can be concluded about the application of FEM in soft robotics: (i) FEM simulation can measure the large deformation that is associated with inflation and deflation. (ii) FEM can identify the performance of the actuator concerning various inputs and analyze rapid and efficient design strategy which reduces cost and time. (iii) for fatigue performance analysis, it is important to calculate stress concentration and strain distribution in a soft actuator. All these features can be achieved through the FEM simulation process. (iv) Moreover, FEM can handle contact nonlinearities that comply with environmental interaction [37] [38] [39].

Material	Shore Hardness	Elongation at Break (%)	Model	Constants	Ref.
Ecoflex 30	00-30	900	Yeoh	$C_1=12.7\text{kPa}$ , $C_2=423\text{Pa}$ , $C_3=-1.46\text{Pa}$	40
Ecoflex 50	00-50	980	Yeoh	$C_1=0.019$ , $C_2=0.009$ , $C_3=-4.75 \times 10^{-6} \text{MPa}$	41
DragonSkin 10	10A	1000	Neo-Hookean	$C_1=0.0426\text{MPa}$	42
DragonSkin 30	30A	364	Ogden	$\mu_1=75.5\text{KPa}$ $\alpha_1=5.84\text{kpa}$	43
Elastosil M4601	28A	700	Yeoh	$C_1=0.11$ , $C_2=0.02\text{MPa}$	44
Smooth-Sil 950	50A	320	Neo-Hookean	$C_1=0.34\text{MPa}$	45
NinjaFlex	85A	660	Generalized Rivlin	$C_{10}=0.233$ , $C_{01}=2.562$ , $C_{20}=0.116$	46
FilaFlex	82A	700	Generalized Rivlin	$C_{10}=-0.4889$ , $C_{01}=0.7147$ , $C_{11}=-0.0044\text{MPa}$	47
Agilus30	30-35A	220-270	Generalized Rivlin	$C_{10}=-0.2704$ , $C_{01}=0.7174$ , $C_{20}=0.07927$ , $C_{11}=-0.2704$ , $C_{02}=0.4709$ , $D_1=0.4574\text{MPa}$	48

Table 5: Mechanical properties and hyperplastic model parameters for popular soft robotic materials.

Silicone rubbers are the most common materials for the fabrication of soft pneumatic actuators. The main reason behind this selection is that they are highly flexible and can undergo a large deformation during high pressure. Hyperplastic models are used for the characterization of soft robotic behavior modeling. For silicone rubber, it is assumed that the material is isotropic and incompressible, and the viscoelasticity and stress-softening are neglected.

Most of soft pneumatic robot has a bending motion that can be approximated as multiple tangent constant sections or small piecewise structures. However, the piecewise constant curvature is applicable when the inertia effect is not countable because it has a very low speed and mass [49]. There are few models such as the Euler\_bernoulli equation [50] [51] and Cosserat rodes [52] are considered to the actuator and the external loading.

### **3.1.3 Material Testing:**

It is important to consider the coefficients in the hyperplastic models for material testing. All of the coefficients such as uniaxial, biaxial, and shear test data are determined by hyperplastic models [53]. Moreover, most of the studies are considered to use uniaxial testing due to their high availability. To observe the behavior of the elastomers, it is obvious to calculate the multiaxial stress states where the pressure of actuators is very important.

In this experiment, the Yeoh model has been used for the actuator characterization concerning different pressure. The Yeoh model can predict elastic behavior with a large range of stress and strain. From this model, it is easy to observe the stress-stretch mechanism in different deformation modes. The main problem of the Ogden model is that this model uses a limited number of testing data like uniaxial tension and the testing of elastomers is not defined properly by international standards. However, the ASTM D142 process has been recommended for uniaxial tensile testing. Furthermore, there are several guidelines that are suggested by Miller:

For the uniaxial tensile test, the specimen must be at least ten times longer than the thickness.

For the shear tests, the specimen should be ten times wider than the length.

For the Biaxial tests, it is recommended to follow the full description of the deformation modes of the elastomer.

All tests should be performed at strain levels related to the application, etc.

## **FEM Simulation Result:**

### **3.1.4 FEM Software:**

The FE simulations were done in the ANSYS Workbench platform, and the method was Static Structural Analysis. For any kind of simulation, the model was imported to “Design Modeler”. The model offers different hyper-elastic material models and ideal performance for the static simulation.

### **3.1.5 Material Model:**

The average experimental stress-strain data were imported and used to define in the model identification as “Uniaxial Test Data” for “Hyperelastic Experimental Data”. For model “Yeoh” was chosen for the perfect fit for experimental data such as Mooney-Rivlin, Ogden, and Neo-Hookean.

### **3.1.6 Meshing**

For FE simulation, it is important to declare the mesh density. The 3D-designed models of the soft actuators meshed with tetrahedral elements. To obtain a specific element size a sizing function was used. The soft actuator models do not need fine mesh density as it is highly deformable. All the mesh size is properly studied and checked that the solution is not dependent on it.

### **3.1.7 Analysis Settings**

For the analysis setting, “Large Deformation” is enabled for the simulations to get the deflections. Moreover, the “Sub steps” of 20 are applied for the simulation to the load gradually. Sub steps are a very important parameter because it prevents the load from being applied

### 3.1.8 Contacts

Frictional contacts are defined as between the walls and surfaces which contact with deformation. Symmetric behavior and optimization show more accurate results and realistic behavior. The “Augmented Lagrange” function is used since it is perfect for frictional and self-contacts. Fixed support conditions are applied to fix the actuator hollow, and the surface area is opened to create negative pressure.

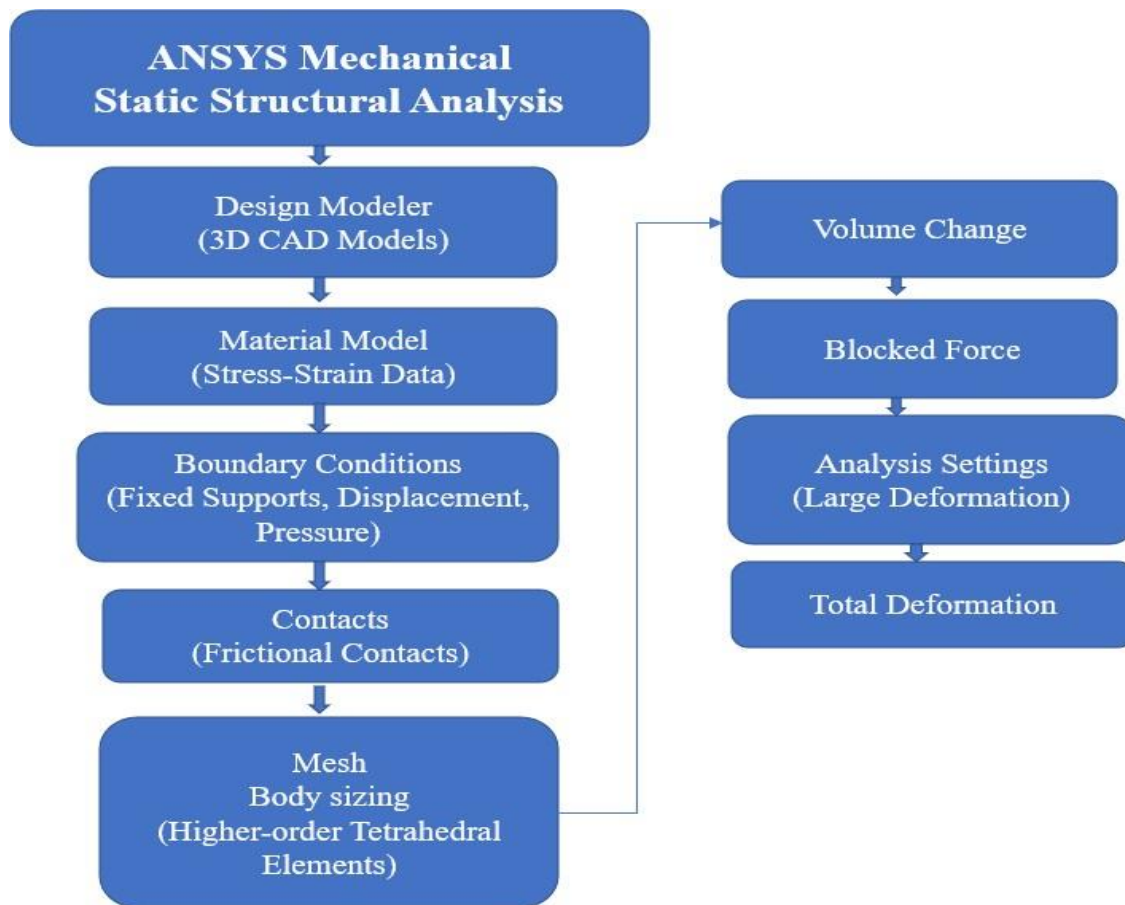
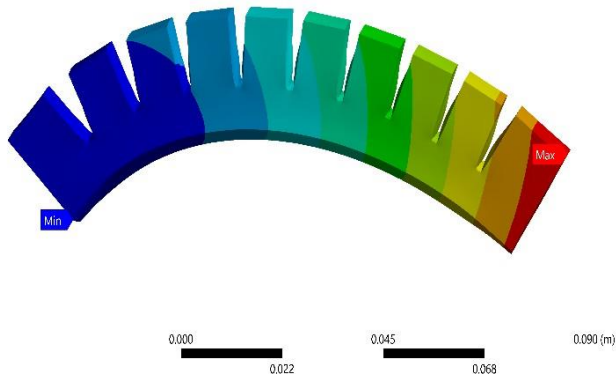


Fig 4: Flowchart of FEM simulation for Pneumatic soft robotic gripper.

**A: Static Structural**  
Total Deformation  
Type: Total Deformation  
Unit: m  
Time: 1  
9/1/2022 6:54 PM

0.094023 Max  
0.083576  
0.073129  
0.062682  
0.052235  
0.041788  
0.031341  
0.020894  
0.010447  
0 Min



**A: Static Structural**  
Total Deformation  
Type: Total Deformation  
Unit: m  
Time: 1  
9/2/2022 4:54 PM

0.13996 Max  
0.12441  
0.10886  
0.093304  
0.077754  
0.062203  
0.046652  
0.031101  
0.015551  
0 Min

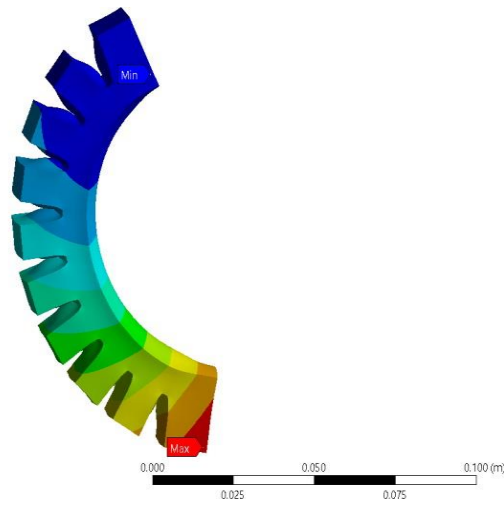


Fig 5: FEM simulation for the soft pneumatic gripper (based on YEOH hyperplastic material model). The deformation result is at 30KPa.

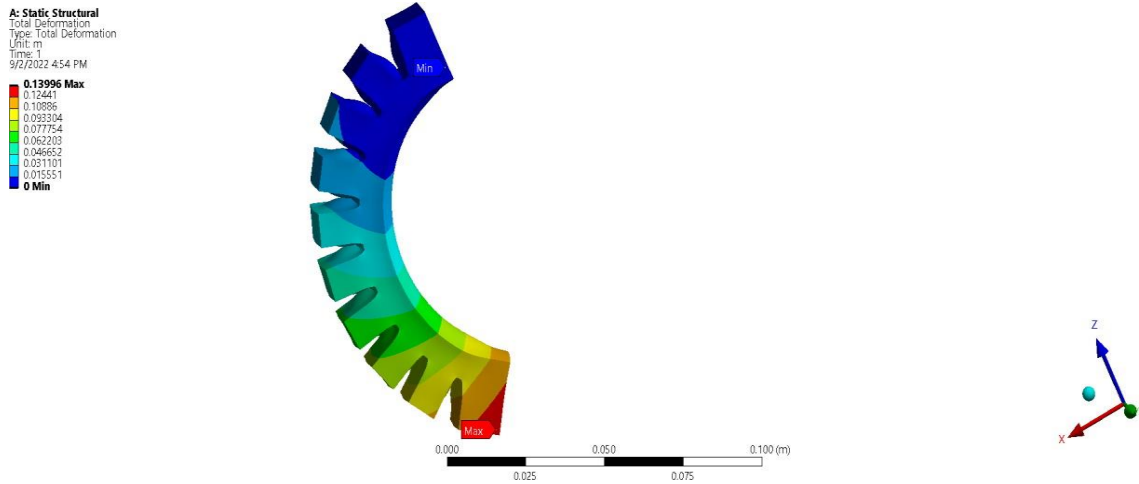


Fig 5: FEM simulation for the soft pneumatic gripper (based on YEOH hyperplastic material model). The deformation result is at 50KPa.

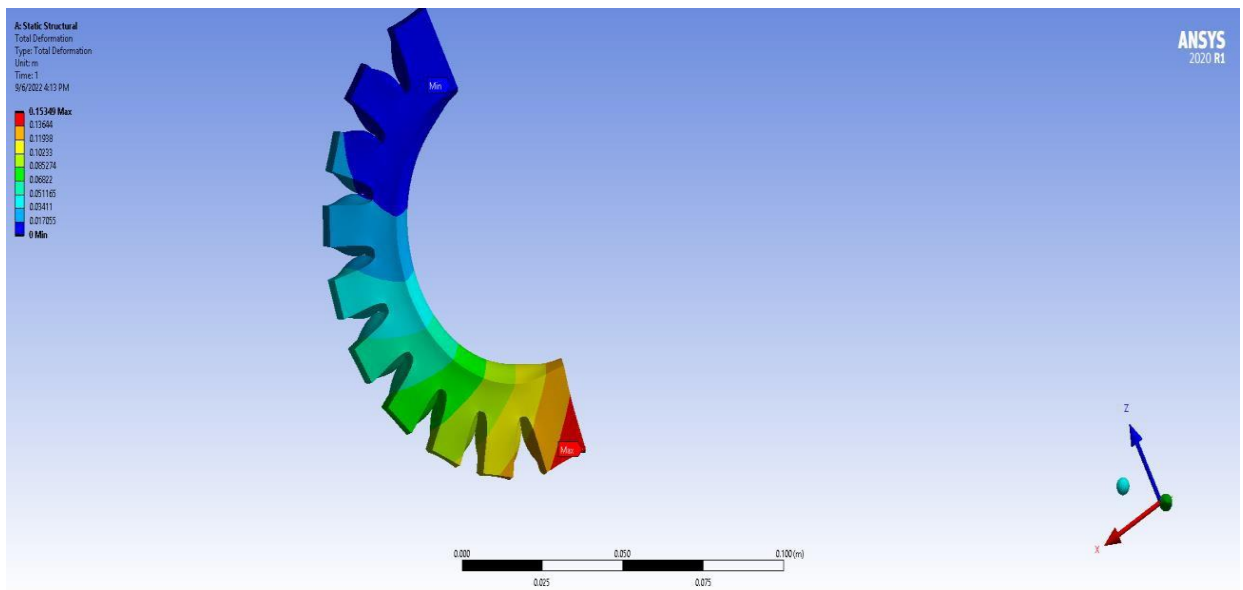


Fig 6: FEM simulation for the soft pneumatic gripper (based on YEOH hyperplastic material model). The deformation result is at 100KPa.

In this work, a computational Finite Element method (FEM) is created to observe the performance of the soft pneumatic actuator. At first, the actuator is designed using Autodesk (Fusion-360) and the geometry is described properly for the analysis. To determine of their geometrical parameters and supplementary materials, tests such as blocked force and displacement are done using the FEM computational modeling. The characterization and inputs are commanded in the ANSYS simulator. This modeling tool can automate different simulation parameters such as part, interactions, meshing, and boundary conditions with respect to command. Additionally, the computational model has enabled to make the design iteration prior to the actual fabrication of the prototypes.

For FEM simulation, ANSYS has been widely used to capture the dynamic response. The simulation software is also capable of providing both dynamic and quasi-static solutions for a different kind of blocked force and displacement of the actuator. It is essential to speed up the explicit solution to perform quasi-static simulations as it maintains the dynamic equilibrium. However, the loading rate needs to be 1% of the acceleration of the stress wave. The airflow inside the actuator is designed as the chambers are disregarded and modeled so that the pressure is equally distributed on the inside of the actuator's internal surfaces. The air pressure is designed for the smooth ramp step to the desired value. In this experiment, a computational model has been developed for the soft pneumatic actuator, including the observed stiffing, contracting, elongating, and bending characteristics. From the FEM simulations, different contour plots have been obtained with respect to different applied pressure. Moreover, the pneumatic soft actuator can bend in one direction when air pressure is applied through for simulation, and a 10-node quadratic, hybrid and constant pressure mesh is generated. One side of the SPA with the adapter is fixed and the static pressure on the surface is generated orthogonally and channels with a closed continuum model. The computed steps are defined under gravity influences, and it is directed perpendicular to gravity. This step is counted for the initial reference coordinates where the pressure is calculated.



The contact interactions between the walls of each chamber are defined by the self-contact and the frictionless surface-to-surface method.

### 3.2. Sensor Design:

#### 3.2.1 Design and Fabrication Methodology:

The total resistance of the flexible sensor depends on the geometry of the sensor. The value of resistivity changes when the sensor is stretched or changes of any physical parameter. According to resistance law,

$$R = \rho \left( \frac{l}{a} \right) \text{----- (1)}$$

$R_0$ = the initial resistance of the sensor.

$\rho$  = represents the electrical resistivity of the liquid metal.

$a$ =cross section area of the sensor.

$l$ = length of the sensor.

If the sensor is stretched or pressure is applied of the sensor, the physical parameter changes. If their lengths become  $l_1$  and  $l_2$  and the cross-section area respectively  $a_0$  and  $a_1$ . Then the total resistance of the sensor can be expressed by:

$$R = \rho \left( \frac{l_1}{a_0} \right) + \rho \left( \frac{l_2}{a_1} \right) \text{----- (2)}$$

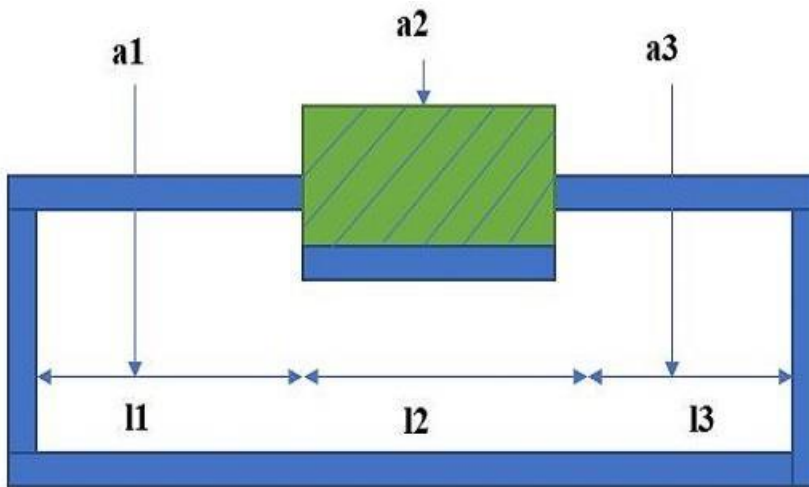


Fig 7: Longitudinal cross-section under pressure.  $l_1$  and  $l_2$  and the cross-section area respectively  $a_0$  and  $a_1$

The resistance change  $\Delta R$  before and after the sensor is extruded can be defined by:

$$R = \left[ \rho \left( \frac{l_1}{a_0} \right) + \rho \left( \frac{l_2}{a_1} \right) \right] - \left[ \rho \left( \frac{l_1+l_2}{a_0} \right) \right] \text{ --- (3)}$$

The change of resistance is dependent on the length and the cross-sectional area of the channel. As a result, to measure the sensor resistance it is very important to consider the length and the cross-sectional area of the sensor properly.

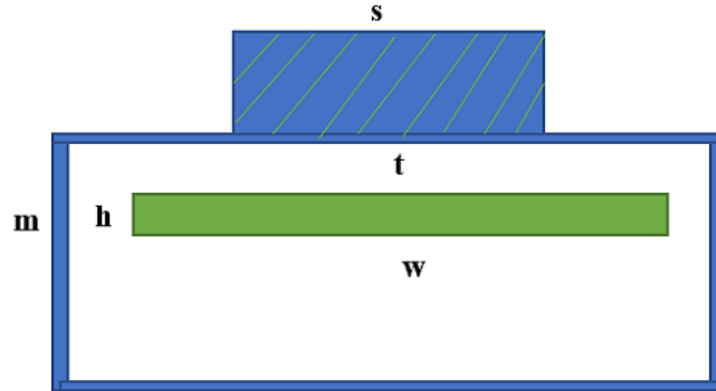


Fig 8: Cross-section view of the sensor.

To get good sensitivity, it is important to investigate the relative size of the sensor from the applied force. Fig 8 represents the lower half of the pressor sensor that contains width  $w$ , height  $h$ , length  $l$  and, the wall thickness  $t$  of the embedded channel. The width of the microchannel is very narrow with respect to actual production with the application layer.

When the struts are wider than the channel, the pressure from the struts will be distributed around the channel and compress the nearest elastomer. According to the Kramers study, when the pressure  $P$  is applied to the upper surface of the elastomer half-space pillar containing the microchannel of conducting liquid. Then the relative resistance can be defined as:

$$\frac{\Delta R}{R_0} = [1 - (\frac{bh1}{2np})^{-1}] \text{-----} (4)$$

However,  $R_0 = \frac{\rho\lambda}{nh1}$  is the initial resistance without deformation, here  $\rho$  = represents the resistivity

of the liquid metal and  $b$  is the bending modulus. If the pressure is  $p$ , then then the equation of  $p$  can be described as:

$$\Delta R = \frac{\rho\lambda}{nh} [(\frac{2np}{bhm\lambda})^{-1} - 1] \text{-----} (5)$$

The physical structure of the sensor has a great influence on its performance. This sensor is mainly two layers: the bottom layer and the top layer. For making, the bottom layer of the sensor is designed using a computer-aided design tool.

### 3.2.3 Device Working Mechanism:

This flexible and stretchable sensor operates based on a deformability-dependent resistive sensing mechanism, which can be described by Equation:

$$\Delta R = (R - R_0) \dots \dots \dots (7)$$

$$\Delta R = \rho \frac{(l + \Delta l)}{(w + \Delta w)} - \rho \frac{l}{wh} \dots \dots \dots (8)$$

The equation shows the apparent resistivity change of the stretchable sensor. Here,

R=the base resistance of the microchannel when there is no stretch.

R<sub>0</sub> = the value of resistance when the sensor is stretched.

ρ = represents the electrical resistivity of the Galinstan.

l = the length of the microchannel.

Δl = the channel length when the sensor is stretched.

w= the width of the sensor.

h= cross-section of the microchannel.

The surface of the devices is stretched when the microfluidic channel experiences the applied pressure on it and deformation occurs. The deformation leads to a decrease in the cross-sectional

area and helps to increase the channel length. As a result, the value of resistance increases across the microfluidic channel.

When the pressure was released, the microfluidic channel recovers soon and goes back to its original state due to the elastic property of the Ecoflex. At the same time, the value of resistance goes to the initial value. In this way, the sensor exhibits an increase and decrease in the electrical resistance of the Galinstan corresponding to the characteristic response of different mechanical forces. The liquid metal-based flexible and stretchable sensor shows different types of distinctive features such as superior thinness, flexibility, small size, and comfortability. It is highly deserved that the sensor is effective and robust and the microchannel sensor should be a high degree of flexibility, conformability, and stretchability. Few physical characteristics such as stretching, bending and twisting are important for sensor application.

In order to measure the performance of the flexible sensor, the applied pressure distribution of the Galinstan-based microchannel sensor corresponding to stretching, bending, and twisting is analyzed. At the stretch conditions, the pressure is distributed uniformly. The sensors show up to 200% stretchability even under high-stress conditions. However, the microchannel shows almost linear behavior concerning applied pressure. That makes the relationship between deformation and resistance change. As a result, the sensor doesn't function failures to high-stress fatigue damage. To evaluate the performance of the sensor, the device is handled meticulously for the loading test and observe the output of the microchannel.

Sensor types	3D Printer	Materials	Pros (+) and Cons (-)
Resistive	FDM	TPU	+ Non-degradable-Agglomeration.
	FDM	TPU	+ Force and contact-Hysteresis
	SLA	Cilia	+High resolution- Nonlinearity
	Inkjet	Tango Black	+Pressure and shear- High-stress deviation
	FDM	Bioagents/PLA/ABS	+High precision- Post-treatment.
	FDM	PLA/carbon fiber	+Negative Poisson's ratio-Strain shift.
	Extrusion	TPU/silver	+Low cost- adhesion

Capacitive	FDM Extrusion DLW FDM	TPU Ionic gel Nanocrystal TPU/PI-ETPU	+High-sensitivity-Simple geometrics +High Sensitivity-Environmental effects +High Spatial resolution-Coupling Loss +Negative Poissons Ratio-Low stretch
Magnetic	FDM FDM	Copper/ABS Magnetic/ABS	+Non-contact + High Temperature range -Low sensitivity-Environmental effect
Inductive	Inkjet FDM	VisiJet/silver Magnetic/PCL	+ Wireless-Dissolving sacrificial +Linear response-Delamination
Optical	FDM Inkjet FDM	ABS Inkjet FDM	ABS InkOrmo/InkEpo

Table 06: Integrated 3D printing of sensors.

## Chapter 4

### FABRICATION PROCESS OF GRIPPER AND SENSOR

#### 4.1. Fabrication Gripper:



Fig. 9: SLA printed soft robotic gripper.

The soft robotic gripper is printed using stereolithography (SLA) process. SLA is a 3D printing technology that uses UV to dry and cure of the printed object. The main advantages of SLA printing is that we can print intricate geometries including complex internal structure that overcome the problems of traditional manufacturing process.

#### 4.1.1. Optimal Grasping Position:

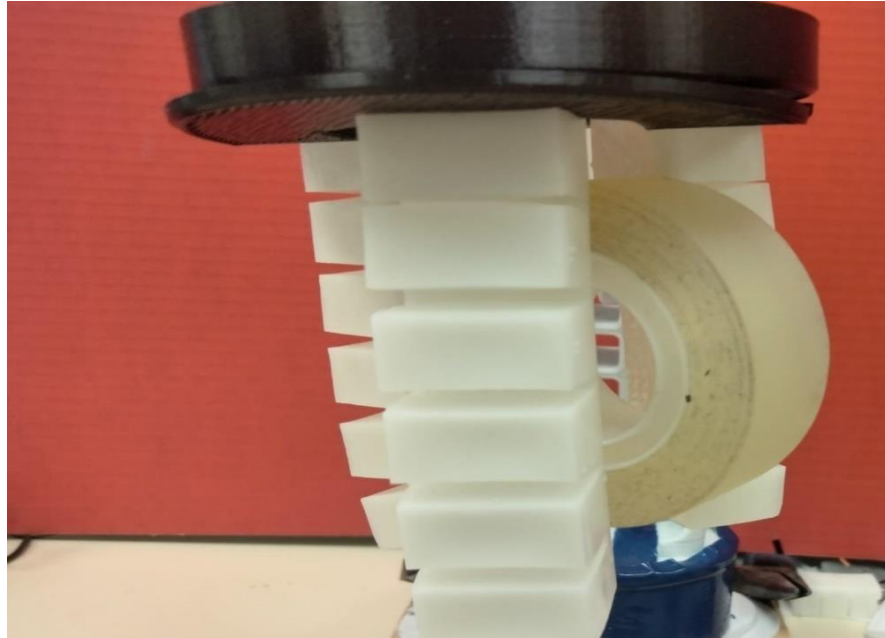


Fig 10: Optimal grasping position of Tape at the applied pressure of 20 KPa

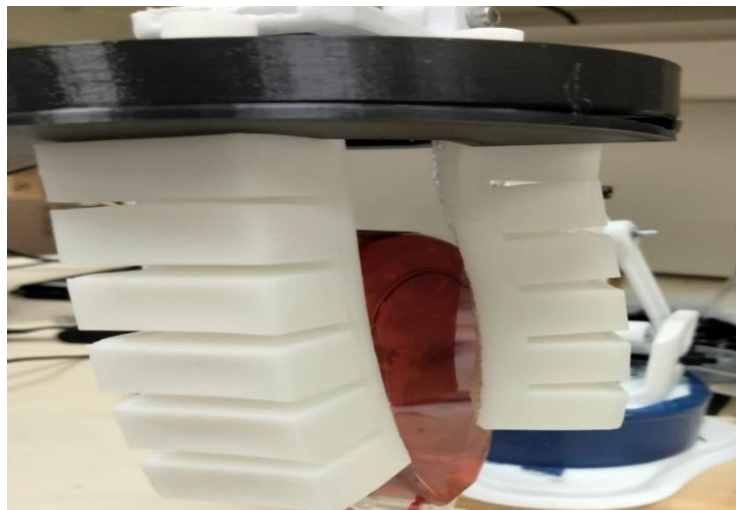


Fig 11: Optimal grasping position of Tape dispenser at the applied pressure of 30 KPa



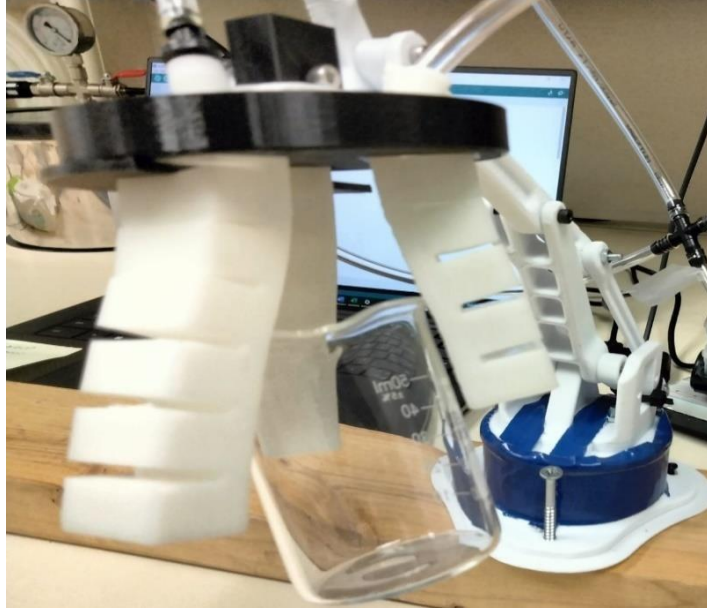


Fig 12: Optimal grasping position of Beaker at the applied pressure of 50 KPa



Fig 13: Optimal grasping position of Orange at the applied pressure of 80 KPa



Fig 14: Optimal grasping position of the Ball at the applied pressure of 100 KPa.

Fig. 10 to Fig. 14 present the optimal grasping position for a soft robotic gripper. For optimal grasping position, five different types of objects whose weight and dimension are different. Here, fig 10 presents the optimal grasping of white tape whose diameter is 20mm and the applied force is 20 KPa. The grasping diameter increase if the applied pressure increase. For example, the diameter of the grasping position increases with respect to 30 KPa, 50 KPa, 80 KPa, and 100 KPa. This is because the bending angle and the output force increase with respect to applied pressure. For a small object like Tape, the gripper cannot vertically take because the bending angle and the output force is comparatively less. Therefore, appropriate pressure can be taken for the optimal holding of an object's different sizes and weights that improve the grasping ability and reliability of the soft gripper.

### 4.1.2: Data collection for Gripper:

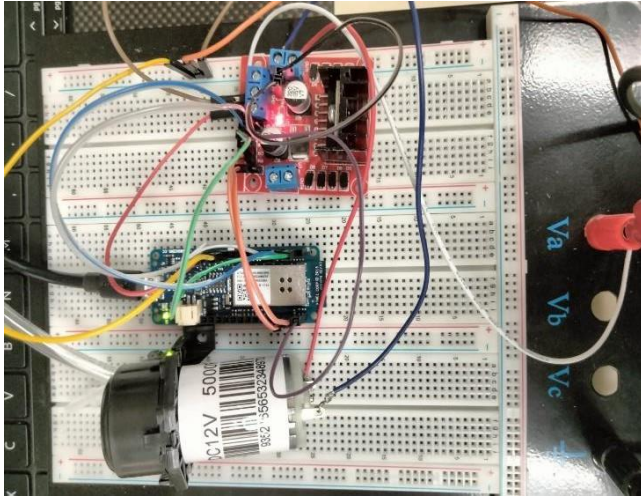


Fig 15: Control unit for the soft robotic gripper.

The laboratory setup is made to check the deformation and grasping ability of the gripper. For the airflow, the peristaltic pump is used. In this setup, air pressure can be applied between 0 to 100 KPa. The actuator has supported the way that it can hang perpendicular to gravity. The pressure is continuously applied from 5 KPa per step. For this experiment, Arduino MKR 1000, Peristaltic pump, L298N motor controller, 12V DC supply voltage, PVC tube hose and pressure sensor were used to accomplish the job.

### 4.2. Liquid Metal Preparation:

Galinstan is a liquid metal that is a combination of gallium, indium, and tin. Their composition ratio is 68.5% Ga, 21.5% In, and 10.0% Sn (by weight). Liquid metal alloys like Galinstan are often used for different sensor applications as well as some computer hardware applications.

Properties	Galinstan
Melting point/°C	-19

Boiling point/°C	>1300
Vapor pressure/mmHg	<10 <sup>-8</sup> at 500 °C
Specific Heat/kJ.kg <sup>-1</sup> °C <sup>-1</sup>	0.200
Density/kgm <sup>-3</sup>	6440
Thermal	16.5
Surface tension/N.m <sup>-1</sup>	0.718 at 25 °C
Solubility in water	Insoluble
Viscosity/Pa.s	2.4×10 <sup>-3</sup> at 20 °C

Table 07: Thermal properties of Galinstan.

After designing the bottom layer, a microchannel has created for liquid metal. Then the bottom layer is printed via a 3-D printer. The fluidic electrodes are embedded in the silicone rubber.



Fig 15: 3-D design layout of the sensor (Silicone wafer).

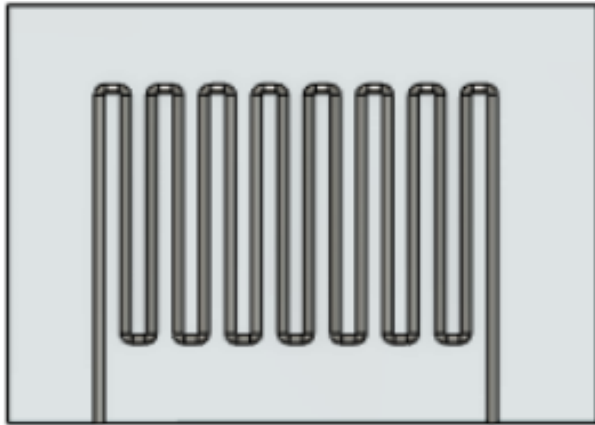


Fig 16: Schematic view of the flexible sensor.

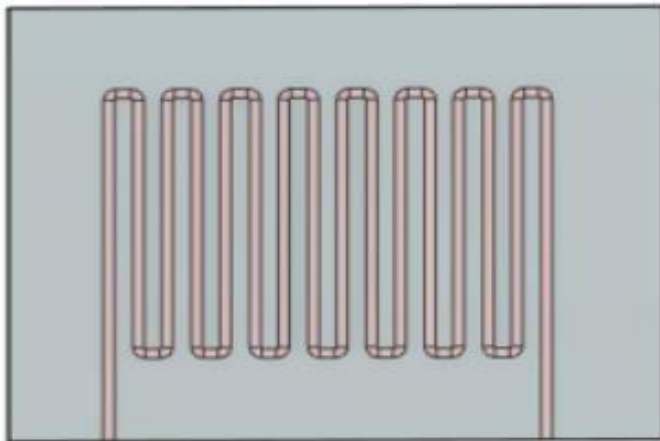


Fig 17: Schematic view of flexible sensor embedded with liquid metal. (Injection of Galinstan)

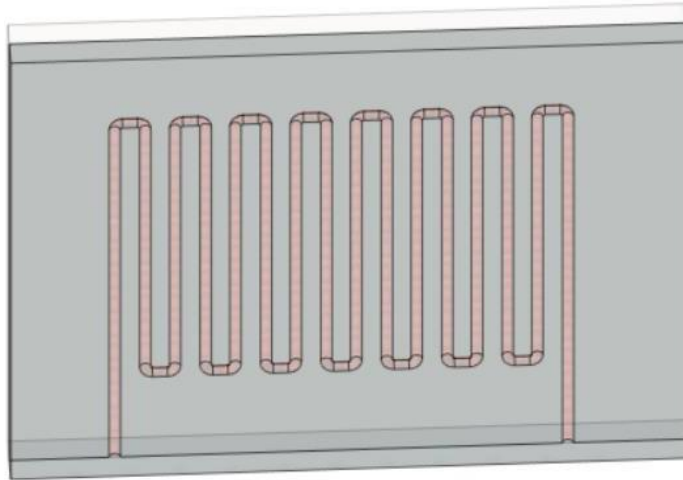


Fig 18: Schematic illustration of the sensor injecting Galinstan inside the channel. (Galinstan Coating)

We use Ecoflex (0050) which has shore hardness =00-50, 100%, tensile module=83 KPa. The top and bottom sealing layers have been used for the dielectric layer. By using the soft elastomer, the concentration between electrodes changes and gives a wide range of resistivity.

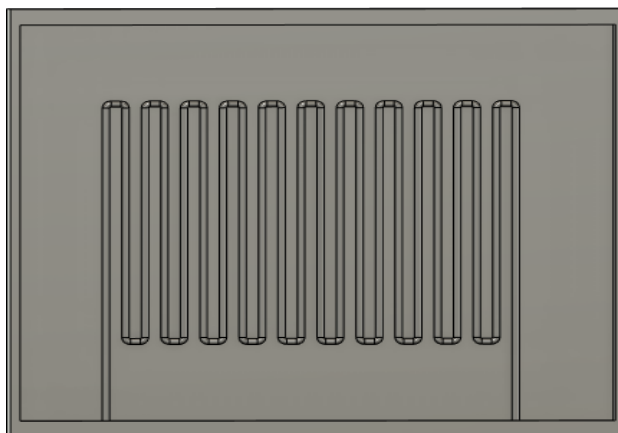


Fig 19: The bottom lid of sensor (pre-mold processing).



Fig 20: Top lid of the sensor for the fabrication process.

#### 4.2.1. Liquid Metal Injection in Microchannel:

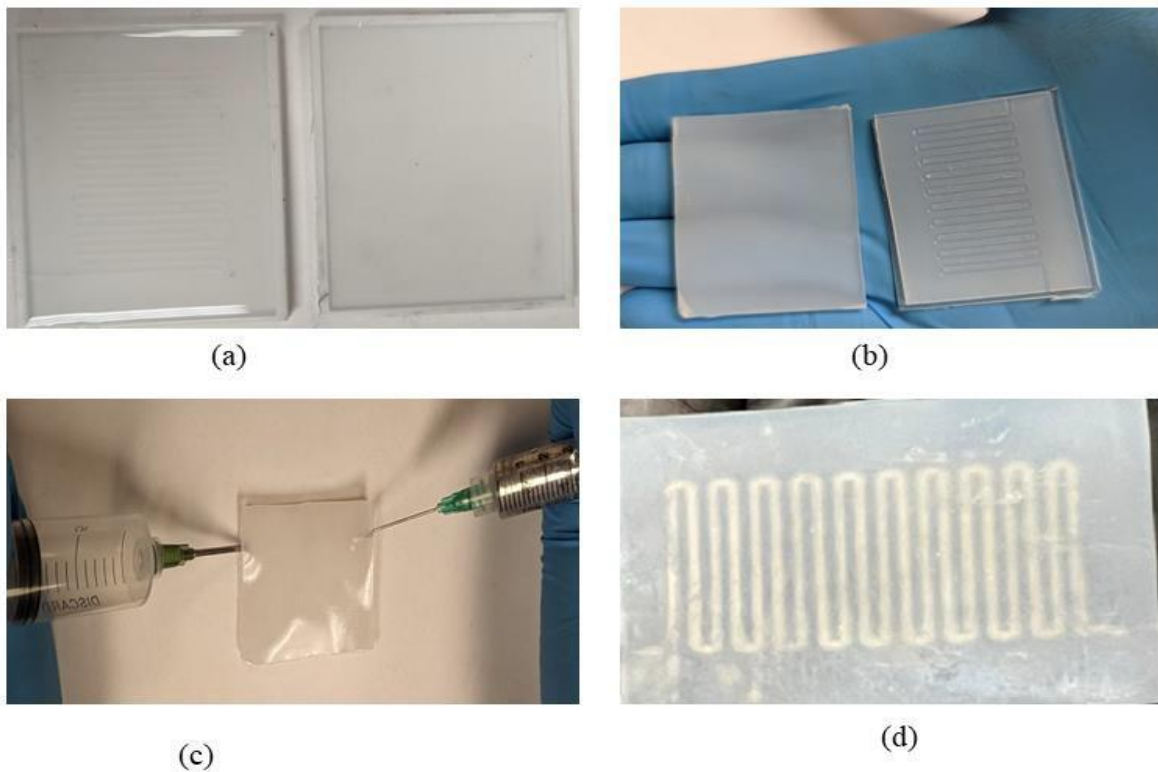


Fig 21: (a) 3-D design layout of the soft sensor, (b) embedded microchannel (c) schematic view of flexible sensor embedded with liquid metal (injection of Galinstan). (d) Schematic illustration of the sensor (Galinstan Coating).

Fig. 21 presents the 3-D design of the soft sensor. The physical design of the bottom and top layers has been demonstrated where the top layer is flat and the microchannel is created in the bottom layer. The Fused Deposition Modeling (FDM) printing method using Ultimaker-3 was used for the mold printing of the sensor. As shown in Fig. 21, the microchannel is created for the injection of liquid metal. The size of the sensor is 30mm×24mm. The fluidic electrodes are embedded in silicone rubber. The top and bottom sealing layers have been used for the dielectric layer. By using the soft elastomer, the concentration between electrodes changes and gives a wide range of resistivity. For this research, Ecoflex (0050) has been used which has shore hardness is 00-50, tensile is 100% and the module is 83 KPa. At first, the elastomer Ecoflex is mixed 1:1 ratio to fabricate the bottom and top layers. A spin coater (KW-4A) is used for the proper mixing of the elastomer. It was rotated using a glass disk at a speed of 1000rpm. Moreover, the important factor is to remove the bubble from the mixer. Otherwise, this might affect the performance of the sensor. A degas chamber (5CFM vacuum, Amazon Inc.) is used to clean the air bubbles. After the degassing process, the silicone is filled in both the top and bottom layers. They are cured for around 4 hours at 80 °C. The mold and bottom layer are separated carefully so that the microchannel becomes unaffected.

Moreover, liquid metal preparation is very challenging as every metal has a different melting temperature. Galinstan is a liquid metal that is a combination of gallium, indium, and tin. Their composition ratio is 68.5% Ga, 21.5% In, and 10.0% Sn (by weight). Liquid metal alloys like Galinstan are often used for different sensor applications as well as some computer hardware applications. At first, the metals were taken in proper ratios and placed in a beaker, and then heat them to 220 °C for almost 1 hour. A glass rod was used during the heating process that helps to mix the metal alloy properly. After melting the metal, they are injected into the micro-channel by using a syringe. For the fabrication process of the soft sensor, a very low amount of Galinstan alloy has been used. Finally, the top layer is aligned carefully with the bottom layer. Again, it is kept for curing properly. Fig. 21 shows the final fabrication of the sensor.





Fig 22: The physical diagram of the preparation process of the liquid metal sensor.



Fig 23: Schematic diagram of the preparation process (stretching condition).



Fig 24: Schematic diagram after fabrication (bending condition).



Fig 25: Image of the fabricated stretchable sensor (thickness).

#### **4.2.2 Data collection for Sensor:**

The data acquisition process is collects data from the sensor and makes a correlation between input and output. Most DAQ devices act as a converter to read from one or more sensors and convert

the reading to a raw measurement value. Many DAQ devices can be scripted to read at various intervals, at particular data rates, etc. In this paper,

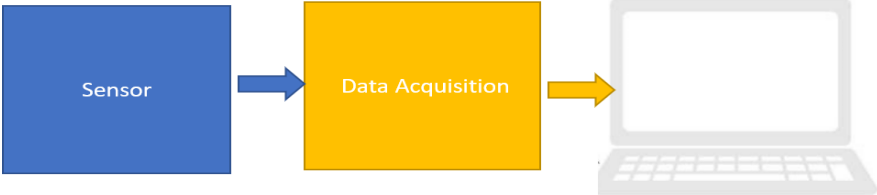


Fig 26: A typical data aquisition process from the sensor.



Fig 27(a): weight used for sensor result validation.

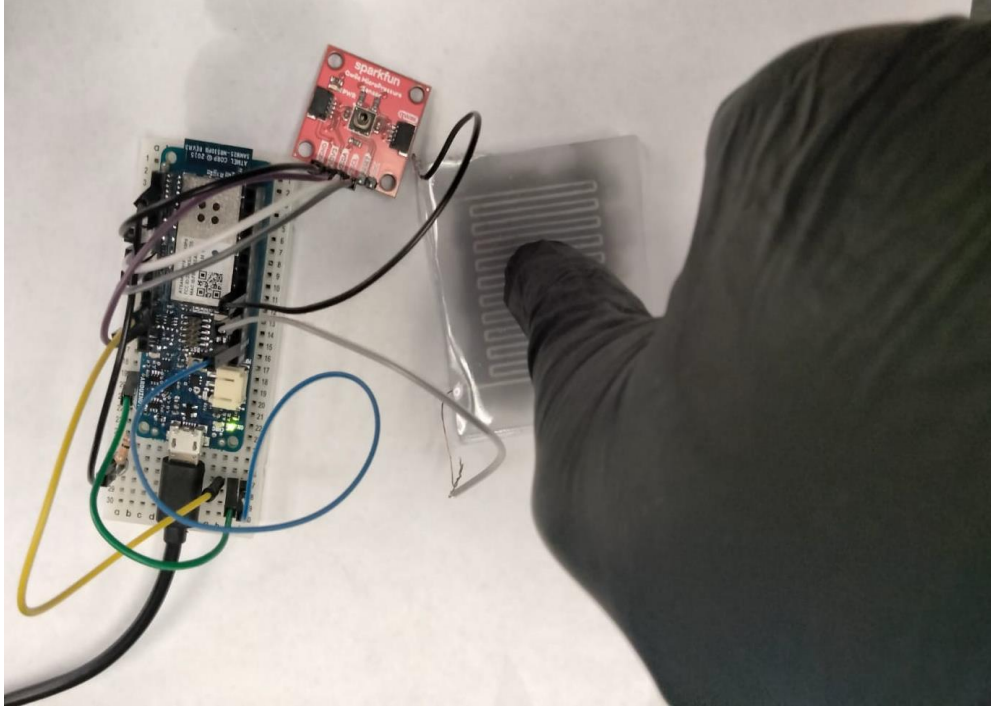


Fig 27(b): sensor response test by creating pressure.

## CHAPTER FIVE

### DISCUSSION, CONCLUSION, FUTURE RESEARCH

#### 5.1. Output Characteristic of Gripper:

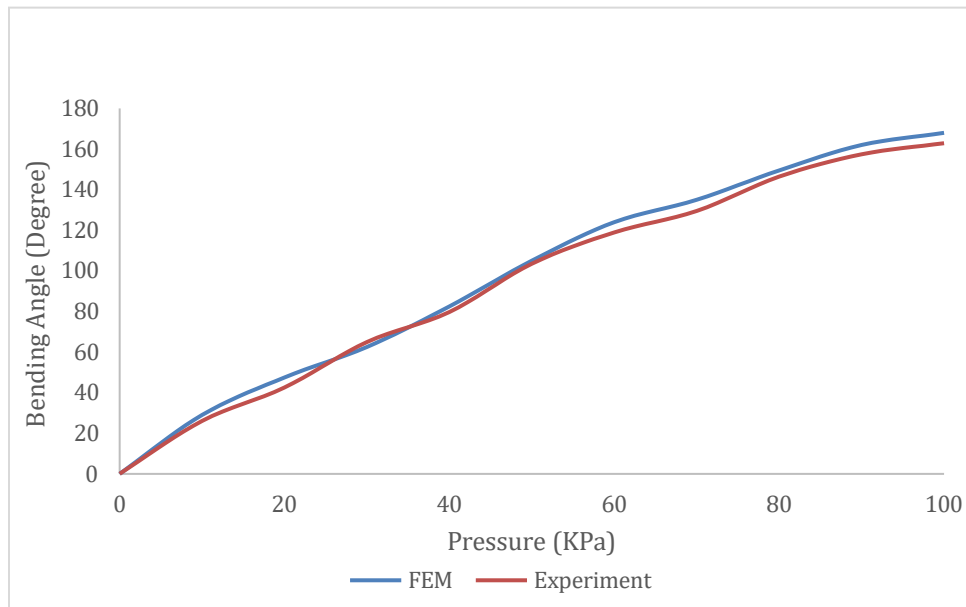


Fig 28: FEM vs Experimental result of bending angle with respect to applied pressure.

The comparison between FE analysis and experiment result is presented in Fig 28. The results show a good comparison between the simulation and experiment results. For the bending angle test, the applied pressure range is 10 to 100 KPa. From the figure, it shows that the starting bending angle is  $28^\circ$  when the applied pressure is 10 KPa and the angle increased linearly. The angle of bending is almost the same at equal pressure. It is obvious that the bending angle increases when the applied pressure increases. The radius of curvature of the actuator also affects the bending angle where the curvature is correlated with pressure. Moreover, when the applied pressure is 100 KPa the bending angle reaches around  $165^\circ$ . Additionally, both the simulation and experimental results show an almost similar trend.

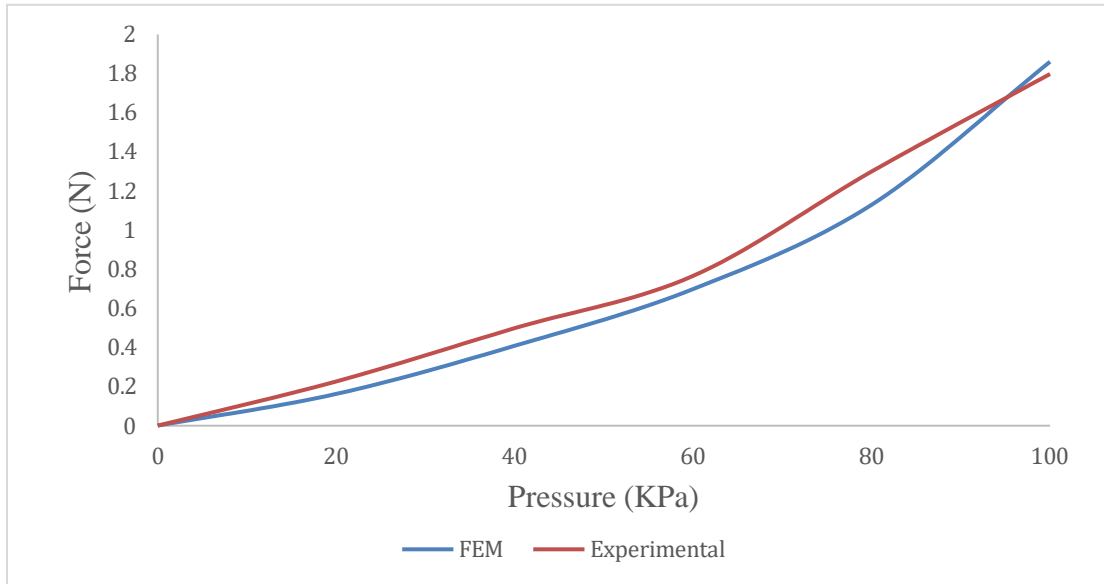


Fig 29: FEM vs Experimental result of load with respect to applied pressure.

As shown in Fig 29, the load with respect to different applied pressure from 10 KPa to 100 KPa. The gripper contacts almost the same length with the applied pressure and the contact force gradually decreases with the chamber position near the tip. From the beginning, there is no substantial change of force. However, there is a very slight change between the simulation and experiment data. When the applied pressure is 20 KPa, the force is .18 N and .2 N respective to FE analysis and experiment.

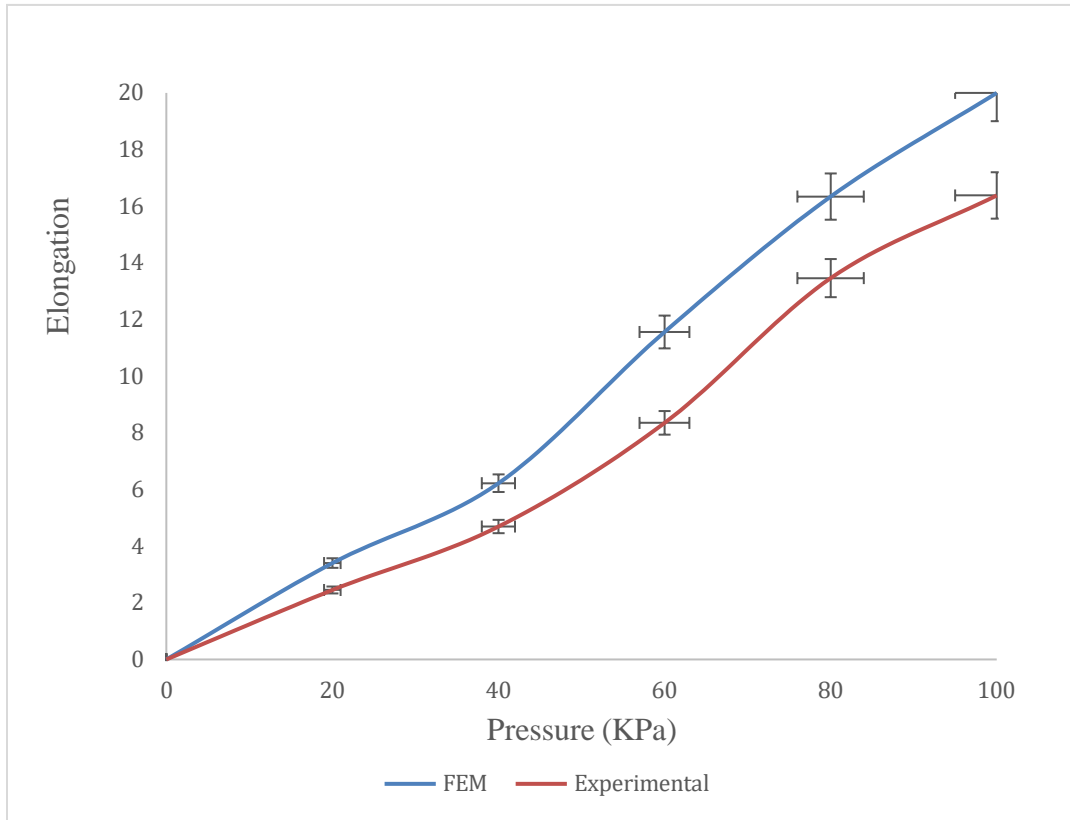


Fig 30: FEM vs Experimental result of elongation with respect to applied pressure.

FEM		Experimental	
Standard Deviation	7.07	Standard Deviation	5.85
Mean	9.60	Mean	7.55

Fig. 30 represents the change of elongation with respect to applied pressure. From the figure, it is evident that there is a slight change between the FEM simulation and the experiment result. At the beginning, it shows the change of elongation is around 1.5 mm when the applied pressure is 20KPa respectively FE and experiment data. The FE simulation result shows linear characteristics where the fabricated gripper did not show such kind of behavior with an increase of applied pressure. When the applied pressure is 100 KPa the value of FE simulation is 20.25 mm and the experimental

The result is 16.50 mm. Though the simulation result is deviated from the experimental result, the fabricated gripper shows reliability and stability during operation.

## **5.2 Output Characteristic of the Sensor:**

The sensor demonstrates prominent mechanical performance which does not represent any structural damage on conditions of high strength. The flexible Galinstan micro channel sensor is designed to accomplish to high mechanical charging though the minimum requirement is not only to high mechanical durability but also high sensitivity. The sensor working mechanism is the resistivity change with respect to the cross-sectional area of the microchannel when the sensor is stretched. The value of resistance becomes larger as the area of the microchannel becomes smaller. It is predominant to execute the design function that is obvious to increase the resistance value and shows an outstanding linear relationship with strain. The sensor demonstrates prominent mechanical performance which does not represent any structural damage in conditions of high strength.

To obtain the output from the sensor different apparatuses have been used for this study. For applying fixed pressure on the sensor, a pressure gauge was used and for storing and analyzing data KEYSIGHT E4089A, Arduino MKR-1000, and MATLAB were used. The flexible Galinstan micro channel sensor is designed to accomplish mechanical changes though the minimum requirement is not only to high mechanical durability but also high sensitivity. The sensor working mechanism is the resistivity change with respect to the cross-sectional area of the micro-channel when the sensor is stretched. The value of resistance becomes larger as the area of the micro-channel becomes smaller. It is predominant to execute the design function that is obvious to increase the resistance value and shows an outstanding linear relationship with strain.

### **5.2.1 : Stretchability:**

Stretchability is one of the primary characteristics of flexible sensors. However, most of the traditional sensors are very rigid and brittle. There might be structural damage and performance failure due to large deformations. The body movements are accommodated by the skin through bending and stretching. The sensor is very stretchable like skin.



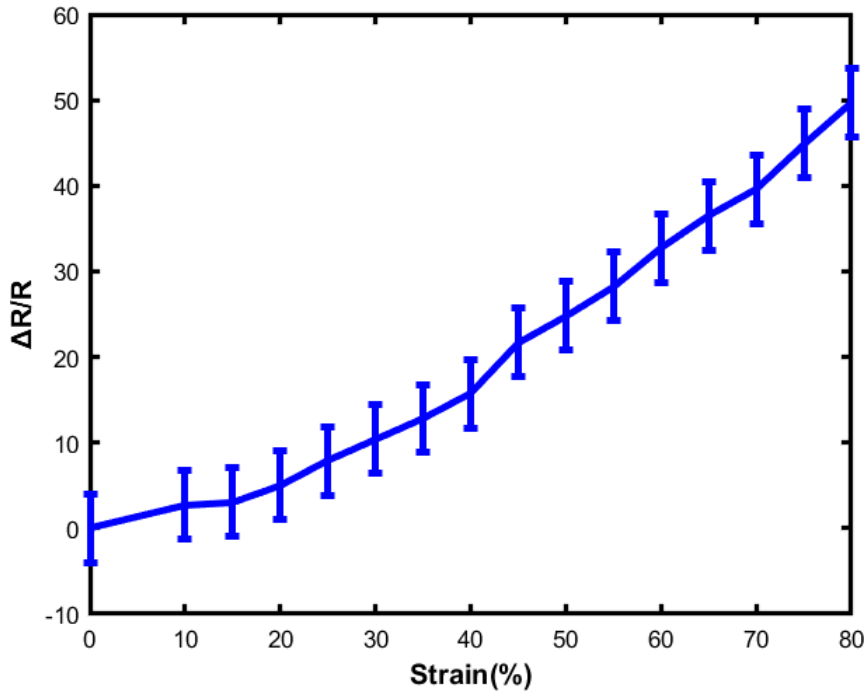


Fig 31: Present the relationship between strain and resistance change (pressure-30kPa).

Elastomer-based flexible resistive strain sensors have different stretchability that depends on their microstructure and sensing component materials. Elastomer-based sensors always present excellent stretchability. Fig.31 represents the relationship between relative resistance change and the strain.

$$\text{Strain} = \frac{(l-l_0)}{l_0} = \frac{\Delta l}{l_0} \quad \text{--- (9)}$$

Here,  $l$  = the length of the sensor before stretched and  $l_0$  = is the value when the sensor is stretched.  $\Delta l$  represents the value of length change at two different environments.

The value of strain is plotted on X-axis and the value of relative resistance change is plotted on Y-axis. Typically, the PDMS/Ecoflex/Elastosil-based sensor's stretchability depends on the physical properties of the material. Sometimes their strain range is 0-10% due to the lack of robust percolating networks of the low aspect ratio. For fabricating this sensor, an Ecoflex 00-50 has been used that helps to become very flexible. Though some research groups used carbon nanotube (CNT) films with highly homogeneous and the result shows microcrack propagation and lateral interconnection. The strain of this sensor can be achieved up to 180% which is applicable for a

wide range of applications. In this investigation, the sensor shows outstanding strain up to 100% and excellent sensitivity. From the Fig 31, the relative resistance change is almost linear and the potential candidate for different applications. Elastomer-based flexible resistive sensor with a different type of stretchability can be used as robotics, artificial skin, and human motion such as breathing, speech, blinks, and bending of joints.

### 5.2.2 : Gauge Factors:

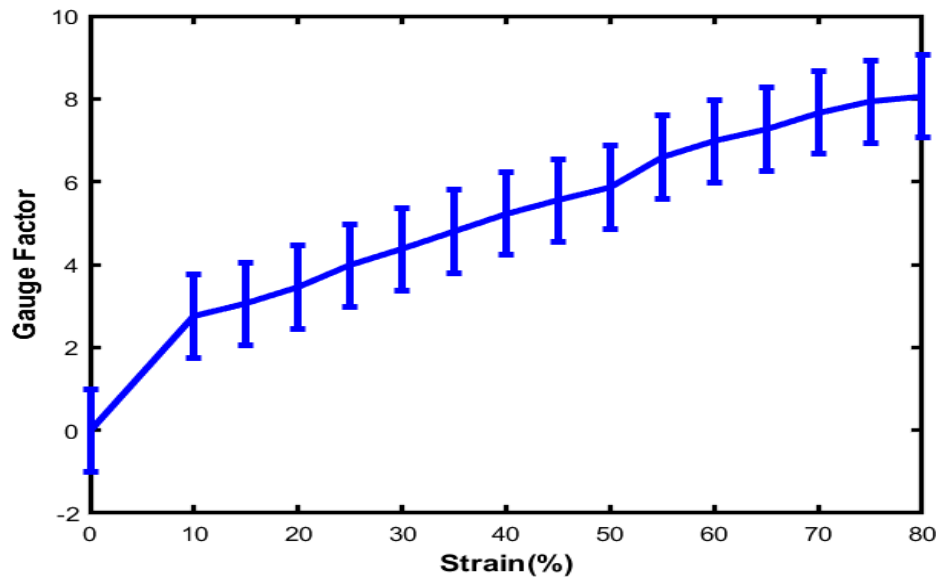


Fig 32: Shows the relationship between the gauge factor and strain.

The gauge factor is one of the important indexes for sensitivity. The gauge factor is defined as:

$$\text{Gauge factor} = \frac{(\Delta R/R)}{\epsilon} \text{ --- (10)}$$

The gauge factor reflects the sensitivity of the flexible sensor, and the slope of the relative resistance change is defined as the gauge factor. The sensor detects very small deformation when the sensor shows a greater gauge factor. Elastomer/Silicone based liquid metal flexible sensors exhibit a gauge factor with a range of 2-20. Moreover, the gauge factor is controlled by the geometry deformation of the liquid metal. Comparative liquid metal, AgNW/PDMS based sensors

have smaller gauge factors of 2-10 and graphene oxide/PDMS based strain sensor exhibits a high gauge factor range of 130-260. According to the graph, the value of the gauge factor reaches around 8.06 when the sensor is stretched to about 80%. The sensors behave identically though there is a slight change of value with a different strain. The linear characteristics indicate that they are a promising candidate for sensor application. From Fig. 32, it is observable that the sensor demonstrated excellent mechanical deformability and did not show any structured damage during mechanical strength changes.

### **5.2.3 : Linearity:**

Linearity is called the percentage of maximum deviation between the calibration curve and the fitting line with full-scale output. Linearity is one of the vital parameters for the sensor application because linearity makes the sensor's signal accurate and is helpful in the follow-up processing of the output signal. Nonlinearity reflects the large deviation between the output signal and the measurement of the parameter. `

As a result, it makes a complicated calibration process and signals distortion which indicates poor performance of the sensitivity. Galinstan/Ecoflex-embedded based sensors typically exhibit linearity and stretchability. Moreover, the cycling test helps to moderate the linearity by stretching/releasing. Fig. 33 represents the relative change of resistance with respect to applied pressure on the soft sensor. The range of applied pressure is 10 kPa to 100 kPa with an increment of 10 kPa. From the graph, it is observed that when the applied pressure is 10Kpa, the relative resistance change is 1.00. However, with the increase in the loading force the value of resistance changed linearly. At 50 kPa applied pressure, the value of relative resistance is 1.81 whereas at 100 kPa applied pressure the value of relative resistance is 2.97. Thus, the results indicate that the sensor provide good dynamic response and stability under different applied pressure

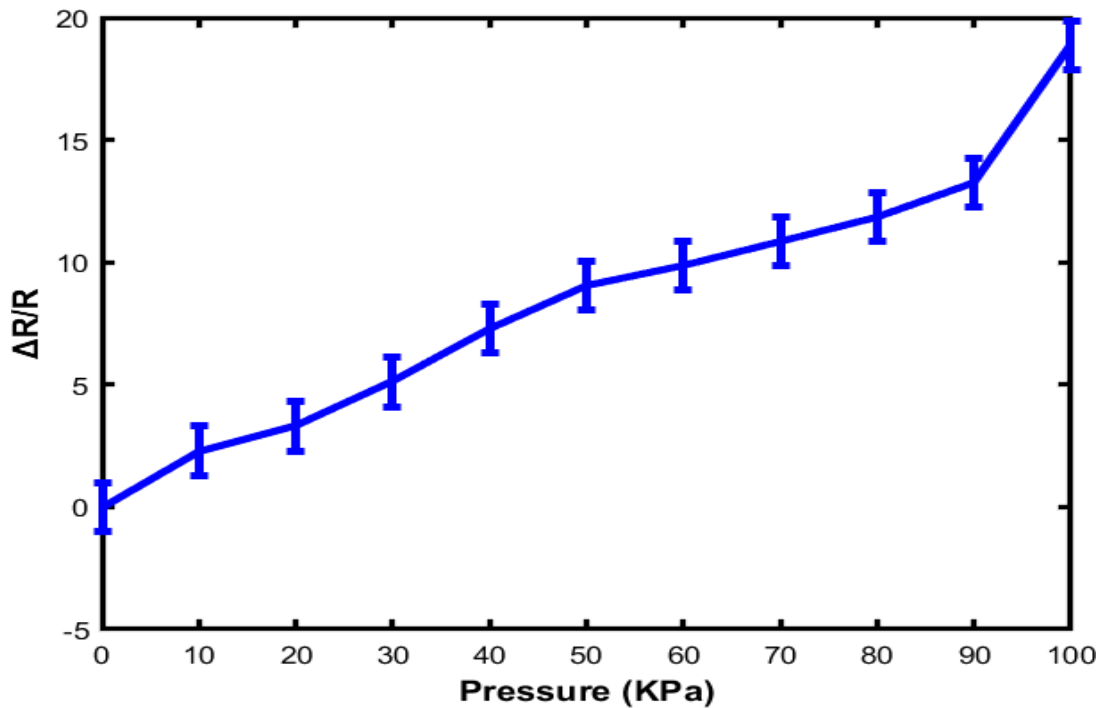


Fig 33: Represents the relative change of resistance with respect to applied pressure.

Typically, the highly sensitive sensor shows strain with nonlinearity and very low stretchability. They always present non-uniform deformation. As a result, the design and fabrication of high linear, stretchable and sensitive sensors still a big challenge till now. In this paper, the fabricated sensor can be used a wide range of applications as it shows moderate linearity and good respond with respect to applied pressure.

### 5.2.4 : Durability

Durability represents the ability of the strain sensor to recover its original properties during the reciprocating deformation. Durability is more important for wearable strain sensors in practical applications due to the inevitability of large, complex, and dynamic strains.

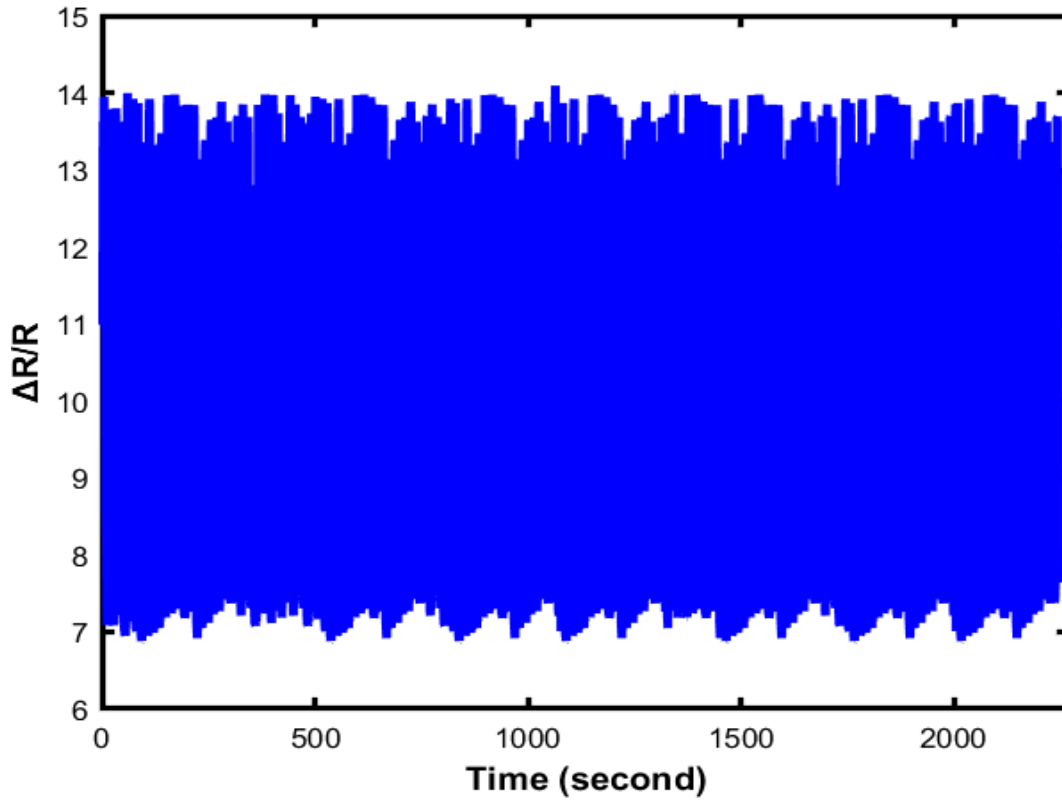


Fig 34: 1000 episodes of cyclic loading and unloading test at 30 kPa up to six minutes.

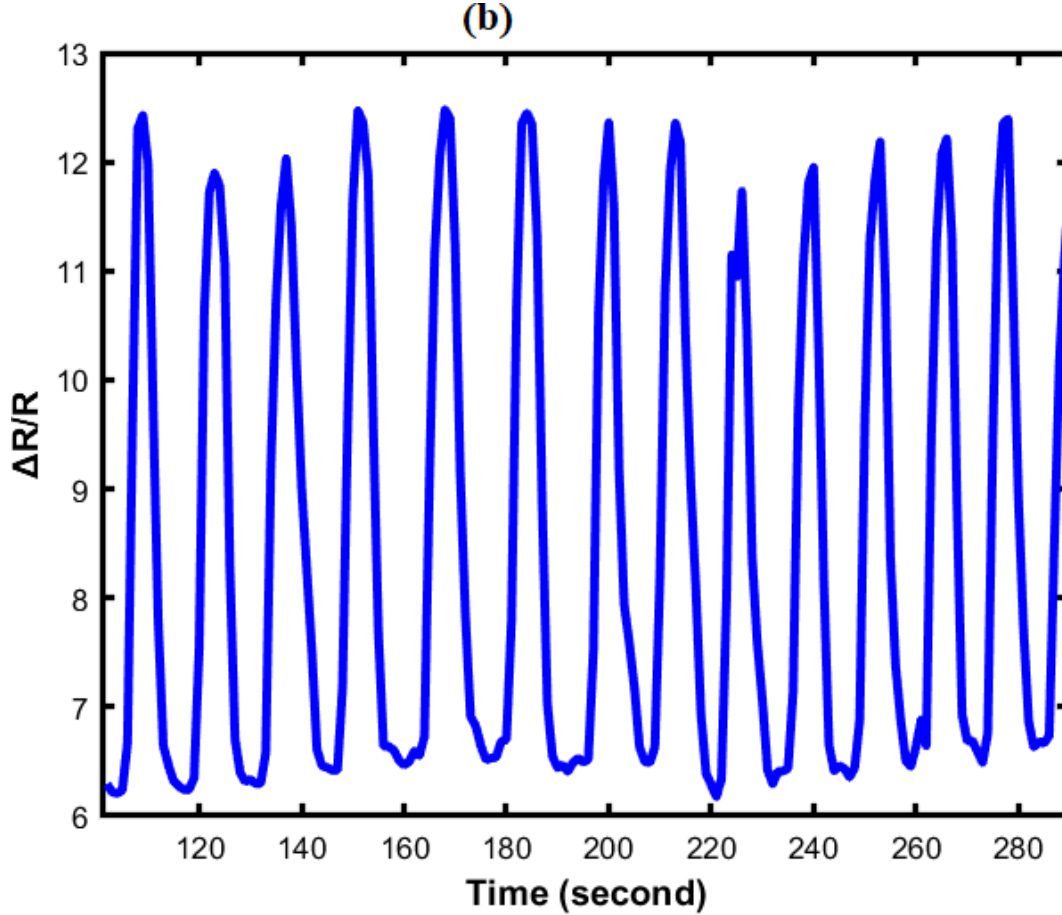


Fig 35: 1000 episodes of cyclic loading and unloading test at 30 kPa (300-second period).

The Galinstan/Ecoflex-based sensor shows long-term reliability during the cycling test with very negligible change in the resistance profile Fig.34) The two-layered flexible sensor shows outstanding dynamic bending stability with an almost constant resistance value where the maximum bending angle was used at 90 degrees. More importantly, the lifetime of the sensor highly depends on the sensor's fabrication. The sensor allows the structure to be repeatedly bent and stretched with superior physical robustness and cyclability. The sensors exhibit high durability that responds to different cyclic loading with remarkable stability even after thousand of cycles of strain ranging from 10%-60%. Fig. 35 presents a thousand episodes of cyclic loading and unloading tests when the applied force is 30kPa. The output of the loading test is generated and plotted. From the

figure, it can be observed that the value of resistance changes repeatedly when the cyclic loading and unloading test occurs. In Fig. 35 enlarged view has been presented of the cyclic test. Thus, the sensor demonstrates good durability and repeatability for long-term application.

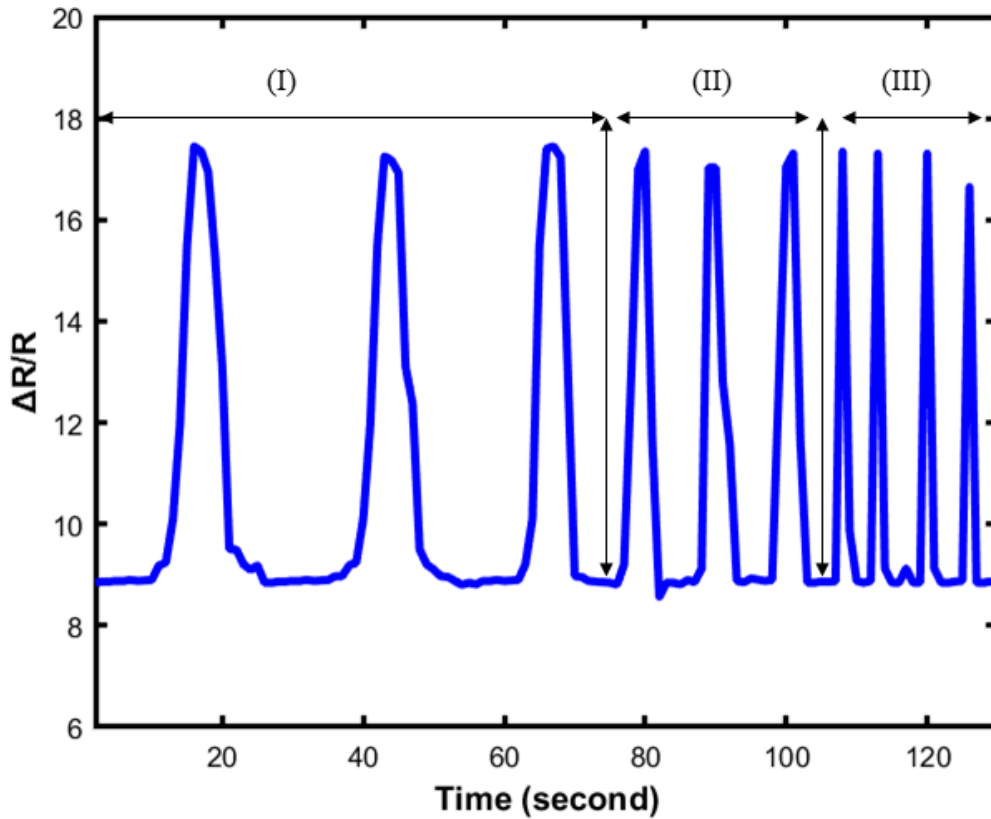


Fig 36: Performance test of the soft sensor using finger positioning.

In Fig. 36 the relative resistance change is observed under different applied frequencies. The loading frequencies are 0.020 Hz, 0.08 Hz, and 0.012 Hz. As shown in Fig. 16, the value of resistance was almost unchanged under applied frequencies which indicates that the sensor is stable under different loading frequencies.



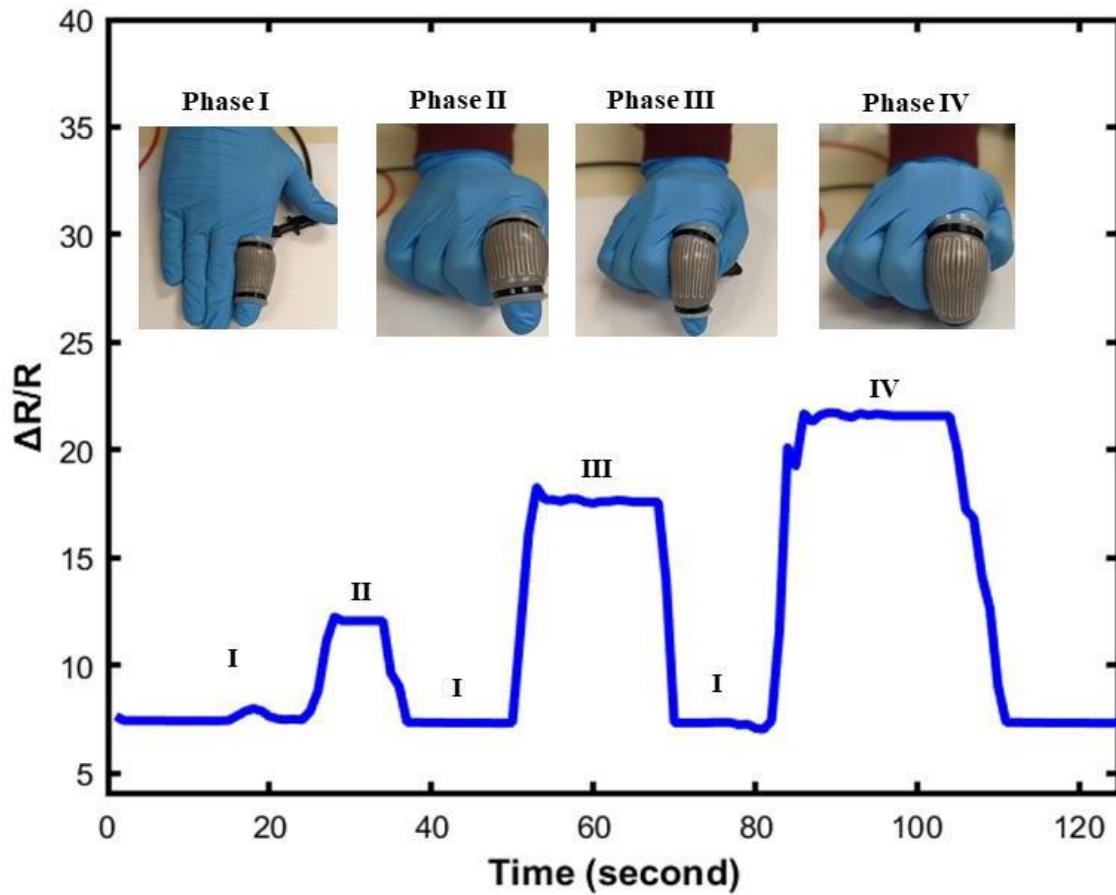


Fig 37: Output feedback of the sensor after creating pressure.

Fig. 37 presents the proof of concept of its application that mainly focused on dynamic responses from the fabricated soft sensor. The sensor can detect different angles and gestures of any object. Fig. 37 shows the change of the resistance value when the sensor is stretched. The result proved that this soft sensor shows outstanding strain performance which easily recognizes the gesture of the hand.

### **5.3: Sensor Application:**

Elastomer-based sensors have a plethora of real-time applications as they exhibit different types of stretchability and comfortability. Some potential application of soft sensor is robotics, artificial skin, health monitoring, and human motion interaction such as breathing, blinks, bending of joints, etc. These types of sensors can be implanted in clothes or directly laminated on human skin which can produce excellent feedback for health monitoring and other activities. Moreover, the potential application of soft sensors is in the soft robotic field. Soft sensors can be used for measuring the direction of the robot, different arm joint angles, the position of objects, etc. These characteristics are applicable to improving the accuracy and control of the robot. Some robotic applications such as grasping, and manipulation are crucial when an attached soft sensor can help to achieve these factors. Overall, the use of soft sensors can enhance the controllability, accuracy, and performance of robots. However, there are still some challenges to the wide application of soft sensors. Most of soft sensors can deform in only one direction and perform one job. Also, these sensors have high modulus materials and weak adhesion structures that might be the reason for comfortless of the users. As a result, they cannot be integrated into the human body for real-time application. Additionally, integration with other devices such as Bluetooth, thin-film batteries, and packaging is a concerning issue for the soft sensor.

#### **5.4. Machine learning model proposition:**

Object detection is a basic visual recognition problem in deep neural networks and computer vision. Visual object detection tries to identify certain classes or objects from a given image. For better quality images, it is very important to collect good cameras and storage devices. But, in this research, we have collected different data from various objects and applied a basic machine-learning algorithm. The common use of the soft sensor is to monitor help or work as a robotic skin. In the same way, we collected data from paper, plants, rose plants, plastic, rubber, floating rubber, and wood. Moreover, as a parameter, we took the height, weight, and width of each object. The resistance values were taken after robotic grasping. With the development of visual recognition based on machine learning has increased its application in diverse fields. However, we collected data using a soft robotic gripper to detect the object size with respect to resistance change and applied different machine learning algorithms to identify the object.

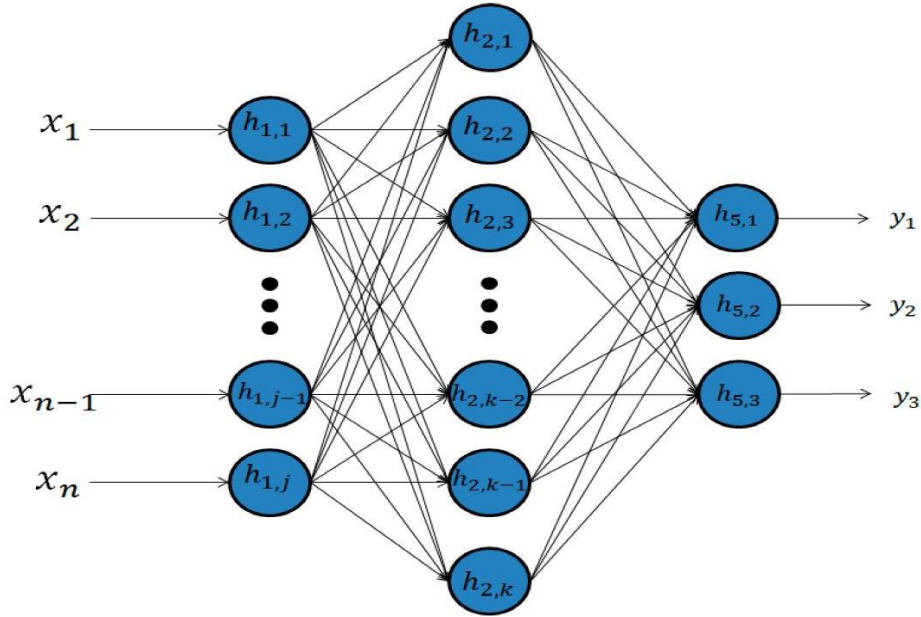


Fig 38: Machine learning architecture.

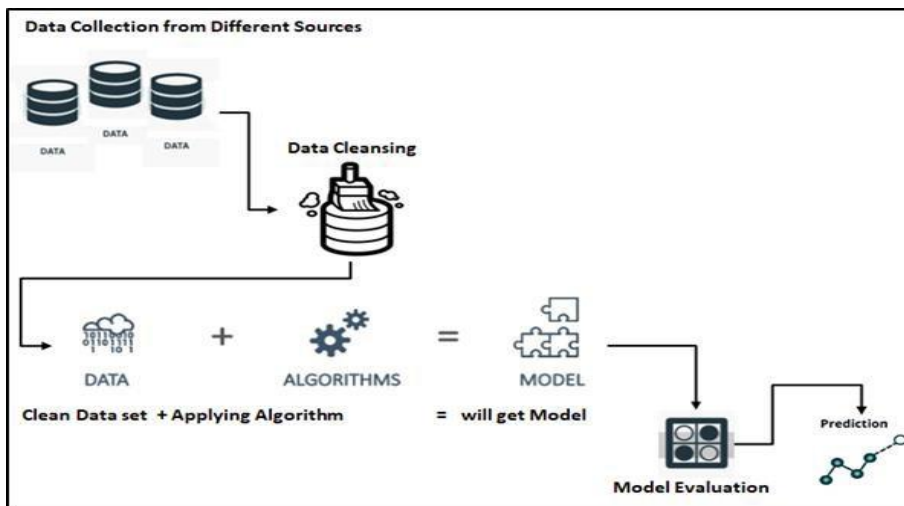


Fig 39: Methodology of the machine learning algorithm.

### 5.4.1. Data Preprocessing:

There are three steps usually followed for different object detection: data collection, feature extraction, and classifier recognition. For this experiment, the dataset is collected from paper,

plants, rose plants, plastic, rubber, floating rubber, and wood. The dataset consists of 295 containing different classes. The number of classification and table is presented in the table:

Class Name	Number of Datasets
Paper	44
Plants	46
Rose plants	46
Plastic	44
Rubber	43
Floating rubber	30
Wood	38

Table 8: The selected group name and the number of datasets

### 5.4.2. Machine Learning:

At first, we calculated the standard error for every feature. From the figure, we can see the standard error is very distinct. The standard error graphs are presented below:

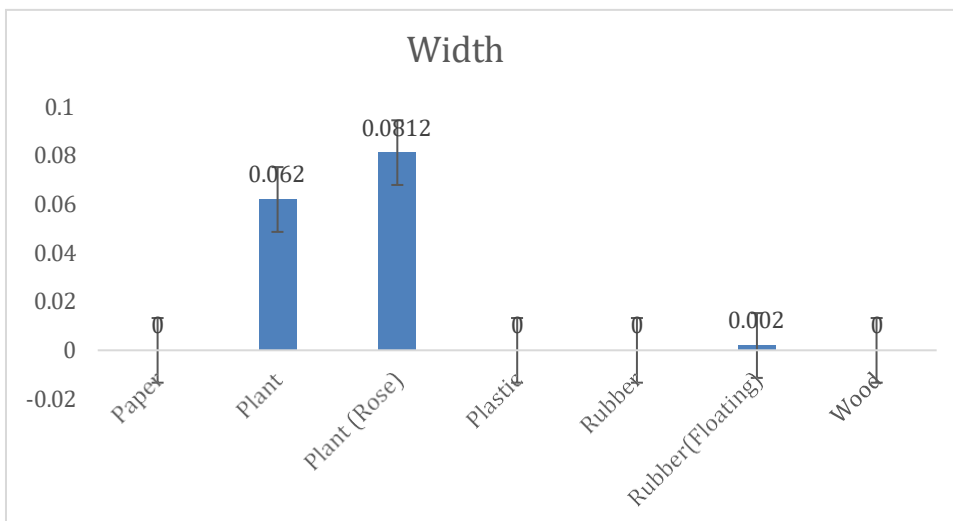


Fig 40: Standard error graph for width.

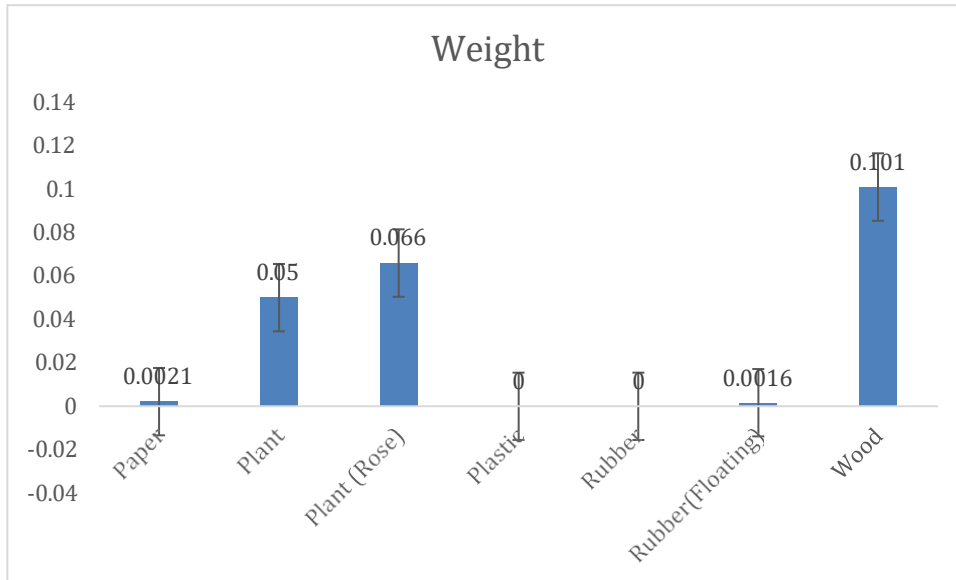


Fig 41: Standard error graph for weight.

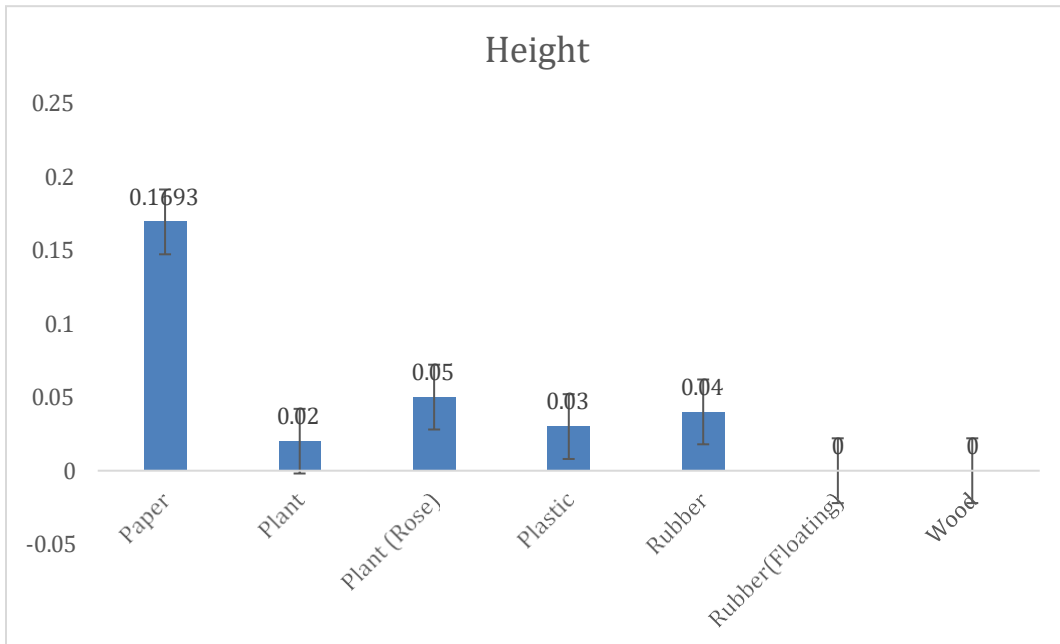


Fig 42: Standard error graph for height.

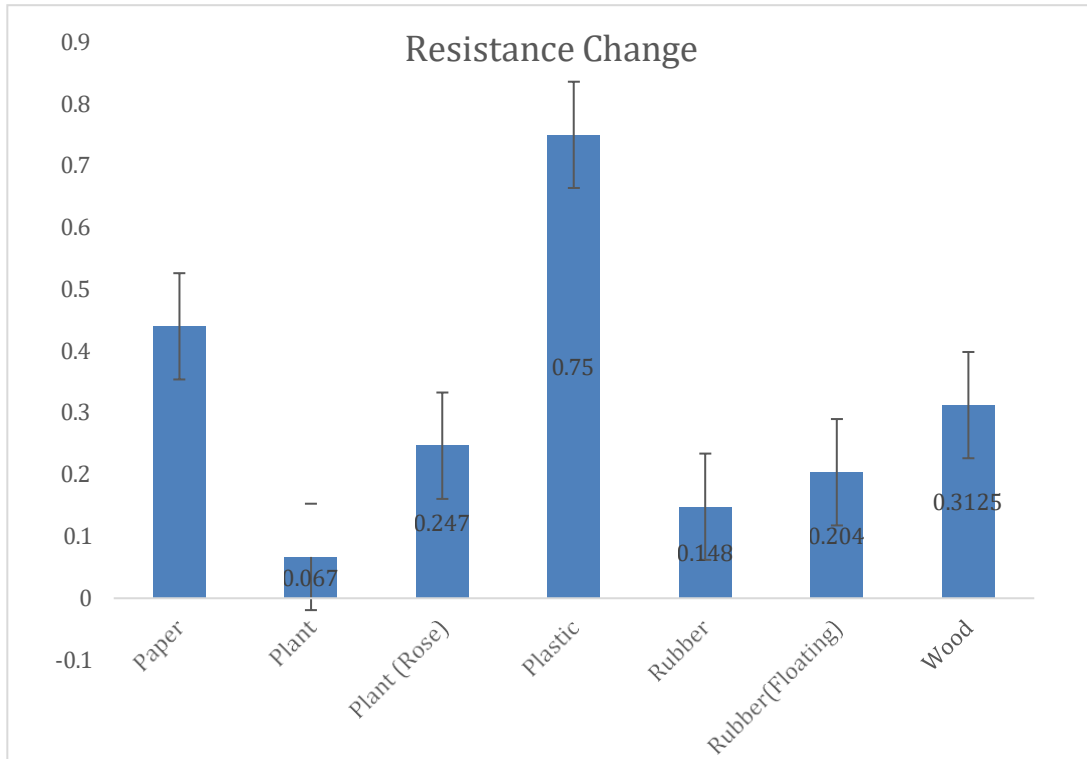


Fig 43: Standard error graph for resistance change.

Fig. 40 to fig. 43 present the standard error for different features such as height, width, weight, and resistance change. From figure, we can see the standard error are separated. However, the standard error for plant is 0.067 which is lowest, and the standard error of plastic is 0.75 which is the highest value for the resistance change. Now, we have trained our data for classification learning to shows the validation of our soft robotic gripper.

		True/Actual	
		Positive	Negative
Predicted	Positive	True Positive	False Positive
	Negative	False Negative	True Negative

Fig 44: The confusion matrix. The result is classified as either true positive, true negative, false positive, or false negative.

In a classification problem, if there are two classes at hand, the actual class is identified by the true positive class, and anything is denoted by the negative class. On the other hand, True Negative is when the class indicates negative, and the actual value is negative. Accordingly, False Positive is when the model falsely predicts while the prediction should be negative and False Negative is when the model predicts the negative when it should be positive.

Moreover, the accuracy of its model is defined by the total correctly predicted samples divided by the total number of predictions provided to the model. The relationship can be defined by the following equation:

$$\text{Accuracy} = \frac{\text{True Positive} + \text{True Negative}}{\text{True Positive} + \text{True Negative} + \text{False Positive} + \text{False Negative}}$$

In contrast, the precision of a model is defined as the number of correctly predicted models divided by the total number of true predictions of a model.

$$\text{Precision} = \frac{\text{True Positive}}{\text{True Positive} + \text{False Positive}}$$

Accordingly, Recall is the ratio between all positive samples in a sample to correctly predicted in a sample. It can be calculated by:



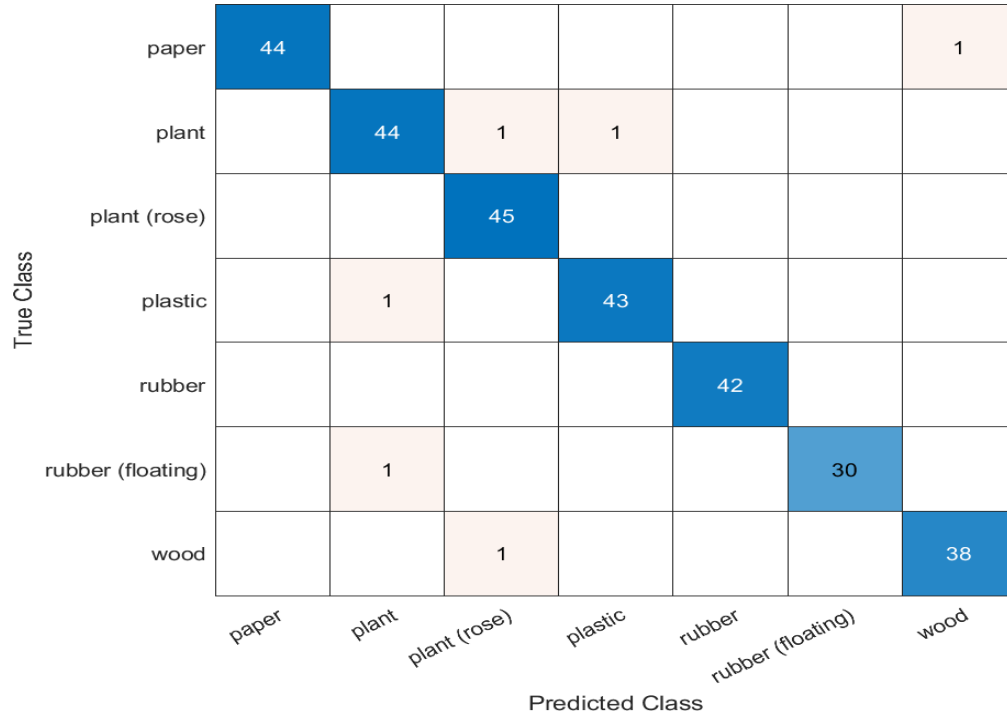


Fig 45: Confusion matrix for Fine tree model.

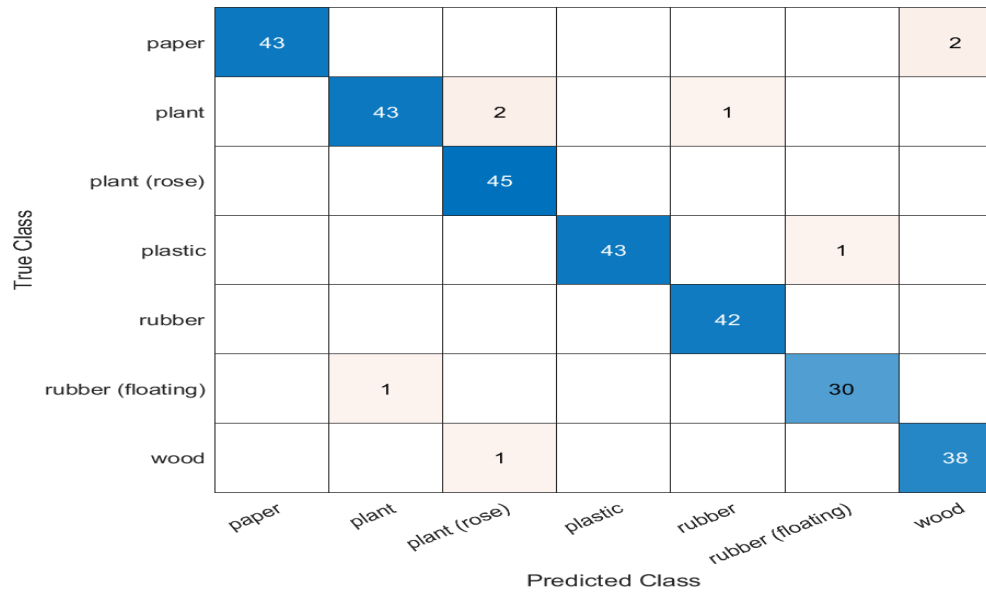


Fig 46: Confusion matrix for ensemble boosted tree model

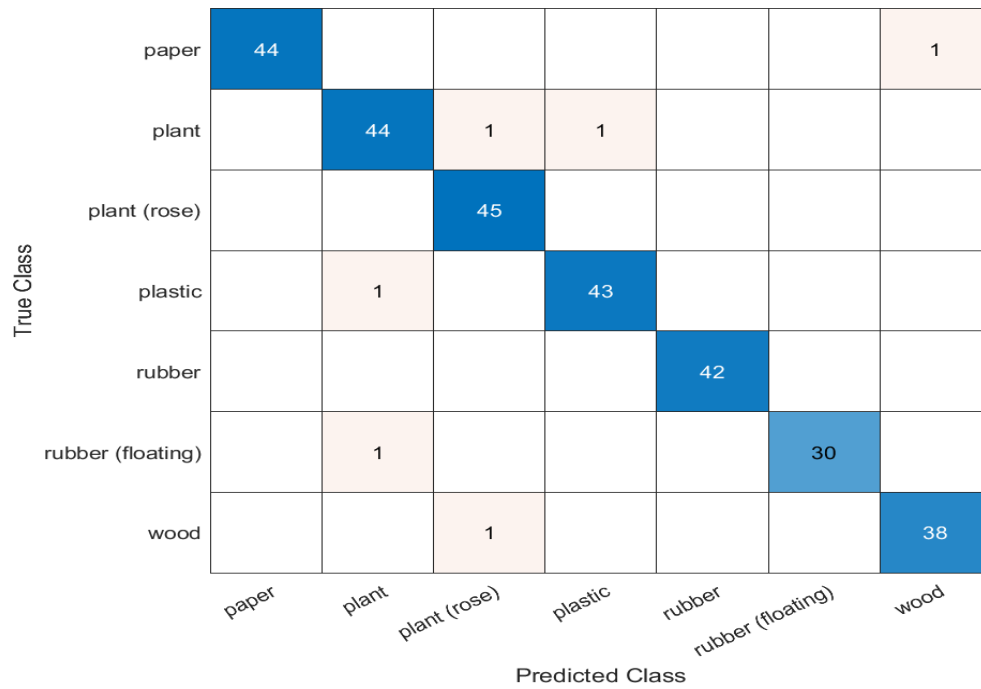


Fig 47: Confusion matrix for ensemble bagged tree model.

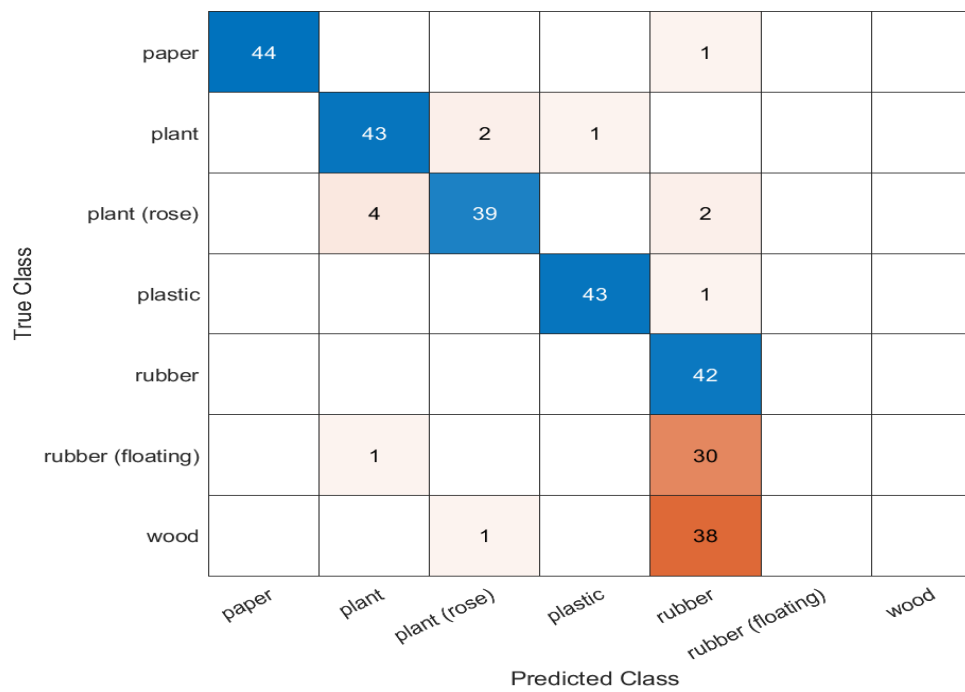


Fig 48: Confusion matrix for SVM model.

Model Name	Accuracy
Ensemble Fine tree	97.90%
Ensemble boosted tree	97.10%
Ensemble bagged tree	97.90%
SVM	72.20%

Table 9: Accuracy of the different classification models.

Different models' confusion matrix is presented in Fig.42 to Fig 45. Among the models, the ensemble fine tree model presents the highest accuracy that is 97.90% and the support vector machine model presents the lowest accuracy which is 72.20%. The accuracy is high because every distinct feature has of the input parameter. Also, the standard error is different from others.

Model Name	Model		
Class Name	Precision (%)	Recall (%)	F1-Score (%)
Paper	97.90	100	98.90
Plants	95	95	95
Rose plants	100	98.00	98.90
Plastic	97.70	97.70	97.70
Rubber	100	100	100
Floating rubber	96.80	100	100
Wood	96.80	97.40	97.40

Table 10: Precision, Recall, and F1 Score of the fine tree model.

Model Name	Model		
Class Name	Precision (%)	Recall (%)	F1-Score (%)
Paper	95.60	100	98.10
Plants	93.50	100	96.60
Rose plants	100	95.80	97.60
Plastic	97.70	100	98.80
Rubber	100	97.70	98.70
Floating rubber	96.80	96.80	96.80
Wood	97.50	95.00	96.20

Table 11: Precision, Recall, and F1 Score of models boosted tree.

Model Name	Model		
Class Name	Precision (%)	Recall (%)	F1-Score (%)
Paper	97.80	100	98.70
Plants	95.70	95.70	95.70
Rose plants	100	97.80	98.90
Plastic	97.70	97.70	97.70
Rubber	100	100	100
Floating rubber	96.80	100	98.60
Wood	97.50	97.50	97.50

Table 12: Precision, Recall, and F1 Score of the bagged tree.

Model Name	Model		
Class Name	Precision (%)	Recall (%)	F1-Score (%)
Paper	97.80	100	98.90
Plants	93.50	89.40	91.60
Rose plants	86.70	92.80	92.30
Plastic	97.70	97.70	97.70
Rubber	100	37.60	54.00
Floating rubber	0	0	0
Wood	0	0	0

Table 13: Precision, Recall, and F1 Score of SVM model.

Table 10 to Table 13 presents the precision, recall, and F1 score of the proposed machine learning model. From Table 10, it can be observed that the highest label of the score was achieved from the rubber and floating rubber object while the plant shows a less score compared to others. Additionally, boosted tree and bagged tree model presents the same kind of result. However, the result is different for the support vector machine model. The highest value of precision is achieved from the rubber, but it shows the lowest recall and F1 scores which are 37.60% and 64.00%. Furthermore, the model is unable to detect the floating rubber and wood.

## 5.5: Conclusion:

This research presents the 3D design, FE analysis, and experimental test for the soft robotic gripper. The FE analysis and experimental results show similar kinds of behavior. The design and fabrication process are described. The experiments showed the characterization of the gripper for experimental research. The gripper was able to manipulate different objects. The grasping experiments show that the soft gripper can hold different weights and sizes of objects with the contact area. Also, a new soft flexible sensor has been introduced. The design, fabrication process, different performance analyses and some potential applications are discussed. There are a plethora of applications of soft sensor such as e-skin, robotics, human-machine interface, health monitoring, sports performance analysis etc. moreover, it can be predicted that wearable soft sensors will play a vital role in our everyday life, especially in health monitoring devices. However, wearable soft sensors in real-life applications still face some challenges. These types of sensors can detect deformation in one direction and multi-direction deformation is still a field of research though few strain and pressure sensors are fabricated and reported. Furthermore, there are a few other obstacles such as high modulation materials and weak adhesion that make the soft sensor not applicable in real life. Overall, this kind of liquid metal sensor shows high performance of stretchability and stability for real-time application. This fabricated sensor can be used in different forcing conditions. The proposed liquid metal sensor can be implanted as a wearable electronics and robotics manipulation application. However, in this research, we have collected different data from various objects and applied classification machine-learning algorithm we collected data from paper, plants, rose plants, plastic, rubber, floating rubber, and wood. The resistance values were taken after robotic grasping. The models show good response with respect to resistance change value. The research presents data collection using a soft robotic gripper and flexible sensor to detect the object size with respect to resistance change and applied different machine learning algorithms to identify the object.

## CHAPTER SIX

### REFERENCES

1. J. Shintake, V. Cacucciolo, D. Floreano, and H. Shea, “Soft robotic grippers,” *Adv. Mater.*, to be published. DOI: 10.1002/adma.201707035.
2. Mohammadi A, Lavranos J, Zhou H, Mutlu R, Alici G, Tan Y, et al. (2020) A practical 3D-printed soft robotic prosthetic hand with multi-articulating capabilities. *PLoS ONE* 15(5): e0232766. <https://doi.org/10.1371/journal.pone.0232766>
3. H. Yap, H. Ng, and C. Yeow, “High-force soft printable pneumatics for soft robotic applications,” *Soft Robot.*, vol. 3, no. 3, pp. 144-158, Sep. 2016.
4. B. Mosadegh, P. Polygerinos, C. Keplinger, S. Wennstedt, R. F. Shepherd, U. Gupta, J. Shim, K. Bertoldi, C. J. Walsh, and G. M. Whitesides, “Pneumatic networks for soft robotics that actuate rapidly,” *Adv. Functional Mater.*, vol. 24, no. 15, pp. 2163–2170, Apr. 2014.
5. G. Alici, T. Canty, R. Mutlu , W. Hu, and V. Sencadas, “Modeling and experimental evaluation of bending behavior of soft pneumatic actuators made of discrete actuation chambers,” *Soft Robot.*, vol. 5, no. 1, pp. 24- 35, Feb. 2018.
6. S. Nikolov, V. Kotev, K. Kostadinov, F. Wang, C. Liang, and Y. Tian, “Model-based design optimization of soft fiber-reinforced bending actuators,” in *Proc. IEEE 3M-NANO.*, Chongqing, China, 2016, pp. 136-140.
7. C. Chun, and B. Hannaford, “Measurement and modeling of McKibben pneumatic artificial muscles,” *IEEE Trans. Robot. and Autom.*, vol. 12, no. 1, pp. 90-102, 1996.
8. S. I. Rich, R. J. Wood, and C. Majidi, “Untethered soft robotics,” *Nature Electron.*, vol. 1, no. 2, pp. 102–112, Feb. 2018.



9. M. Wehner, R. L. Truby, D. J. Fitzgerald, B. Mosadegh, G. M. Whitesides, J. A. Lewis, and R. J. Wood, “An integrated design and fabrication strategy for entirely soft, autonomous robots,” *Nature*, vol. 536, no. 7617, pp. 451–455, Aug. 2016.
10. C. Majidi, “Soft-matter engineering for soft robotics,” *Adv. Mater. Technol.*, vol. 4, no. 2, Dec. 2018, Art. no. 1800477
11. G. Robinson and J. B. C. Davies, “Continuum robots—A state of the art,” in *Proc. IEEE Int. Conf. Robot. Autom.*, vol. 4, May 1999, pp. 2849–2854.
12. D. Trivedi, C. D. Rahn, W. M. Kier, and I. D. Walker, “Soft robotics: Biological inspiration, state of the art, and future research,” *Appl. Bionics Biomech.*, vol. 5, no. 3, pp. 99–117, 2008s.
13. X. Qi, H. Shi, T. Pinto, and X. Tan, “A novel pneumatic soft snake robot using traveling-wave locomotion in constrained environments,” *IEEE Robot. Autom. Lett.*, vol. 5, no. 2, pp. 1610–1617, Apr. 2020.
14. M. Luo, W. Tao, F. Chen, T. K. Khuu, S. Ozel, and C. D. Onal, “Design improvements and dynamic characterization on fluidic elastomer actuators for a soft robotic snake,” in *Proc. IEEE Int. Conf. Technol. Practical Robot. Appl. (TePRA)*, Apr. 2014, pp. 1–6.
15. A. A. Calderón, J. C. Ugalde, J. C. Zagal, and N. O. Pérez-Arancibia, “Design, fabrication and control of a multi-material-multi-actuator soft robot inspired by burrowing worms,” in *Proc. IEEE Int. Conf. Robot. Biomimetics (ROBIO)*, Dec. 2016, pp. 31–38.
16. M. S. Xavier, A. J. Fleming, and Y. K. Yong, “Image-guided locomotion of a pneumatic-driven peristaltic soft robot,” in *Proc. IEEE Int. Conf. Robot. Biomimetics (ROBIO)*, Dec. 2019, pp. 2269–2274.
17. J. Zhang, J. Tang, J. Hong, T. Lu, and H. Wang, “The design and analysis of pneumatic rubber actuator of soft robotic fish,” in *Proc. Int. Conf. Intell. Robot. Appl.*, 2014, pp. 320–327.
18. T. Hou, X. Yang, H. Su, L. Chen, T. Wang, J. Liang, and S. Zhang, “Design, fabrication and morphing mechanism of soft fins and arms of a squid-like aquatic-aerial vehicle with morphology tradeoff,” in *Proc. IEEE Int. Conf. Robot. Biomimetics (ROBIO)*, Dec. 2019, pp. 1020–1026.
19. M. Cianchetti, T. Ranzani, G. Gerboni, T. Nanayakkara, K. Althoefer, P. Dasgupta, and A. Menciassi, “Soft robotics technologies to address shortcomings in today’s minimally

- invasive surgery: The STIFF-FLOP approach,” *Soft Robot.*, vol. 1, no. 2, pp. 122–131, 2014
20. D. O’Brien and D. M. Lane, “3D force control system design for a hydraulic parallel bellows continuum actuator,” in *Proc. IEEE Int. Conf. Robot. Autom.*, vol. 3, May 2001, pp. 2375–2380.
  21. M. S. Xavier, A. J. Fleming, and Y. K. Yong, “Finite element modeling of soft fluidic actuators: Overview and recent developments,” *Adv. Intell. Syst.*, vol. 3, no. 2, Feb. 2021, Art. no. 2000187
  22. F. Chen, W. Xu, H. Zhang, Y. Wang, J. Cao, M. Y. Wang, H. Ren, J. Zhu, and Y. F. Zhang, “Topology optimized design, fabrication, and characterization of a soft cable-driven gripper,” *IEEE Robot. Autom. Lett.*, vol. 3, no. 3, pp. 2463–2470, Jul. 2018..
  23. M. Calisti, M. Giorelli, G. Levy, B. Mazzolai, B. Hochner, C. Laschi, and P. Dario, “An octopus-bioinspired solution to movement and manipulation for soft robots,” *Bioinspiration Biomimetics*, vol. 6, no. 3, Sep. 2011, Art. no. 036002.
  24. W. Wang and S.-H. Ahn, “Shape memory alloy-based soft gripper with variable stiffness for compliant and effective grasping,” *Soft Robot.*, vol. 4, no. 4, pp. 379–389, Dec. 2017.
  25. X. Tang, K. Li, Y. Liu, D. Zhou, and J. Zhao, “A general soft robot module driven by twisted and coiled actuators,” *Smart Mater. Struct.*, vol. 28, no. 3, Mar. 2019, Art. no. 035019.
  26. X. Tang, K. Li, Y. Liu, D. Zhou, and J. Zhao, “A general soft robot module driven by twisted and coiled actuators,” *Smart Mater. Struct.*, vol. 28, no. 3, Mar. 2019, Art. no. 035019.
  27. W. Dou, G. Zhong, J. Cao, Z. Shi, B. Peng, and L. Jiang, “Soft robotic manipulators: Designs, actuation, stiffness tuning, and sensing,” *Adv. Mater. Technol.*, vol. 6, no. 9, Sep. 2021, Art. no. 2100018.
  28. S. Zaidi, M. Maselli, C. Laschi, and M. Cianchetti, “Actuation technologies for soft robot grippers and manipulators: A review,” *Curr. Robot. Rep.*, vol. 2, no. 3, pp. 1–15, 2021.
  29. C. Tawk and G. Alici, “A review of 3D-printable soft pneumatic actuators and sensors: Research challenges and opportunities,” *Adv. Intell. Syst.*, vol. 3, no. 6, Jun. 2021, Art. no. 2000223.

30. M. S. Xavier, C. D. Tawk, Y. K. Yong, and A. J. Fleming, “3D-printed omnidirectional soft pneumatic actuators: Design, modeling and characterization,” *Sens. Actuators A, Phys.*, vol. 332, Dec. 2021, Art. no. 113199.
31. P. Polygerinos, N. Correll, S. A. Morin, B. Mosadegh, C. D. Onal, K. Petersen, M. Cianchetti, M. T. Tolley, and R. F. Shepherd, “Soft robotics: Review of fluid-driven intrinsically soft devices; manufacturing, sensing, control, and applications in human-robot interaction,” *Adv. Eng. Mater.*, vol. 19, no. 12, Dec. 2017, Art. no. 1700016.
32. L. Hines, K. Petersen, G. Z. Lum, and M. Sitti, “Soft actuators for smallscale robotics,” *Adv. Mater.*, vol. 29, no. 13, Apr. 2017, Art. no. 160348.
33. F. Schmitt, O. Piccin, L. Barbé, and B. Bayle, “Soft robots manufacturing: A review,” *Frontiers Robot. AI*, vol. 5, p. 84, Jul. 2018.
34. T. J. Wallin, J. Pikul, and R. F. Shepherd, “3D printing of soft robotic systems,” *Nature Rev. Mater.*, vol. 3, no. 6, pp. 84–100, Jun. 2018.
35. X. Hu, A. Chen, Y. Luo, C. Zhang, and E. Zhang, “Steerable catheters for minimally invasive surgery: A review and future directions,” *Comput. Assist. Surgery*, vol. 23, no. 1, pp. 21–41, Jan. 2018.
36. Y. Elsayed, A. Vincensi, C. Lekakou, T. Geng, C. M. Saaj, T. Ranzani, M. Cianchetti, and A. Menciassi, “Finite element analysis and design optimization of a pneumatically actuating silicone module for robotic surgery applications,” *Soft Robot.*, vol. 1, no. 4, pp. 255–262, Dec. 2014.
37. C. Tawk and G. Alici, “Finite element modeling in the design process of 3D printed pneumatic soft actuators and sensors,” *Robotics*, vol. 9, no. 3, p. 52, Jul. 2020.
38. P. Moseley, J. M. Florez, H. A. Sonar, G. Agarwal, W. Curtin, and J. Paik, “Modeling, design, and development of soft pneumatic actuators with finite element method,” *Adv. Eng. Mater.*, vol. 18, no. 6, pp. 978–988, Jun. 2016.
39. G. Decroly, B. Mertens, P. Lambert, and A. Delchambre, “Design, characterization and optimization of a soft fluidic actuator for minimally invasive surgery,” *Int. J. Comput. Assist. Radiol. Surg.*, vol. 15, no. 2, pp. 333–340, 2019.
40. D. Sarkar, S. Dasgupta, A. Arora, and S. Sen, “A soft bendingtype actuator using hyper-elastic materials: Development, analysis and characterization,” in *Proc. Adv. Robot.*, Jul. 2019, pp. 1–7..

41. P. Polygerinos, K. Galloway, Z. Wang, F. Connolly, and H. Young. (2020). Fiber Reinforced Actuators: Finite Element Modelling. Accessed: Feb. 10, 2019. [Online]. Available: <https://softroboticstoolkit.com/book/fr-modeling>. E. Milana, B. V. Raemdonck, K. Cornelis, E. Dehaerne, J. D. Clerck, Y. D. Groof, T. D. Vil, B. Gorissen, and D. Reynaerts, “EELWORM: A bioinspired multimodal amphibious soft robot,” in Proc. 3rd IEEE Int. Conf. Soft Robot. (RoboSoft), May 2020, pp. 766–771.
42. X. Peng, N. Zhang, L. Ge, and G. Gu, “Dimension optimization of pneumatically actuated soft continuum manipulators,” in Proc. 2nd IEEE Int. Conf. Soft Robot. (RoboSoft), Apr. 2019, pp. 13–18.
43. F. Connolly, C. J. Walsh, and K. Bertoldi, “Automatic design of fiberreinforced soft actuators for trajectory matching,” Proc. Nat. Acad. Sci. USA, vol. 114, no. 1, pp. 51–56, Jan. 2017.
44. C. Tawk, G. M. Spinks, M. Panhuis, and G. Alici, “3D printable linear soft vacuum actuators: Their modeling, performance quantification and application in soft robotic systems,” IEEE/ASME Trans. Mechatronics, vol. 24, no. 5, pp. 2118–2129, Oct. 2019.
45. W. Hu and G. Alici, “Bioinspired three-dimensional-printed helical soft pneumatic actuators and their characterization,” Soft Robot., vol. 7, no. 3, pp. 267–282, Jun. 2020.
46. C. Pasquier, T. Chen, S. Tibbits, and K. Shea, “Design and computational modeling of a 3D printed pneumatic toolkit for soft robotics,” Soft Robot., vol. 6, no. 5, pp. 657–663, Oct. 2019.
47. S. Neppalli, B. Jones, in Proc. IEEE/RSJ IEEE Int. Conf. on Intelligent Robots and Systems, IEEE, Piscataway, NJ 2007, pp. 1503–1507.
48. B. Gorissen, D. Reynaerts, S. Konishi, K. Yoshida, J.-W. Kim, M. De Volder, Adv. Mater. 2017, 29, 43.
49. I. Gravagne, C. Rahn, I. Walker, IEEE/ASME Trans. Mechatron 2003, 8, 229.
50. B. Jones, R. Gray, K. Turlapati, in Proc. IEEE/RSJ IEEE Int. Conf. on Intelligent Robots and Systems, IEEE, Piscataway, NJ 2009, pp. 2659–2664.
51. Bartolozzi, C., Natale, L., Nori, F. *et al.* Robots with a sense of touch. *Nature Mater* **15**, 921–925 (2016). <https://doi.org/10.1038/nmat4731>.
52. Hammock ML, Chortos A, Tee BC, Tok JB, Bao Z. 25th anniversary article: The evolution of electronic skin (e-skin): a brief history, design considerations, and recent progress. Adv

Mater. 2013 Nov 13;25(42):5997-6038. doi: 10.1002/adma.201302240. Epub 2013 Oct 22. PMID: 24151185.

53. Xu S, Zhang Y, Jia L, et al. Soft microfluidic assemblies of sensors, circuits, and radios for the skin. *Science* (New York, N.Y.). 2014 Apr;344(6179):70-74. DOI: 10.1126/science.1250169. PMID: 24700852.
54. Li, Guangyong et al. “A galinstan-based inkjet printing system for highly stretchable electronics with self-healing capability.” *Lab on a chip* 16 8 (2016): 1366-73 .
55. Carmel Majidi, Kaveh Alizadeh, Yunsik Ohm, Andre Silva, Mahmoud Tavakoli, Liquid metal polymer composites: from printed stretchable circuits to soft actuators, *Flexible and Printed Electronics*, 10.1088/2058-8585/ac515a, 7, 1, (013002).
56. Gao, Q. et al. Highly stretchable sensors for wearable biomedical applications. *Journal of Materials Science*, 1–37 (2019).
57. Chossat, J. B., Park, Y. L., Wood, R. J. & Duchaine, V. A Sof Strain Sensor Based on Ionic and Metal Liquids. *IEEE Sensors Journal* 13, 3405–3414 (2013).
58. Yan, S. et al. Liquid metal-based amalgamation-assisted lithography for fabrication of complex channels with diverse structures and configurations. *Lab on A Chip* 18 (2018).
59. Kazem, N., Bartlett, M. D. & Majidi, C. Extreme Toughening of Sof Materials with Liquid Metal. *Advanced Materials* 30, 1706594 (2018).
60. Muth, J. T. et al. Embedded 3D printing of strain sensors within highly stretchable elastomers. *Advanced Materials* 26, 6307–6312 (2014).
61. Kazem, N., Hellebrekers, T. & Majidi, C. Sof Multifunctional Composites and Emulsions with Liquid Metals. *Advanced Materials* 29 (2017).
62. Tang, S. Y. et al. Microfluidic Mass Production of Stabilized and Stealthy Liquid Metal Nanoparticles. *Small* 14 (2018).
63. Tavakoli, M. et al. EGaIn-Assisted Room-Temperature Sintering of Silver Nanoparticles for Stretchable, Inkjet-Printed, Tin-Film Electronics. *Advanced Materials*, 1801852 (2018).
64. Daeneke, Torben et al. “Liquid metals: fundamentals and applications in chemistry.” *Chemical Society reviews* 47 11 (2018): 4073-4111.

65. Dickey, Michael David et al. “Eutectic Gallium-Indium (EGaIn): A Liquid Metal Alloy for the Formation of Stable Structures in Microchannels at Room Temperature.” *Advanced Functional Materials* 18 (2008): n.
66. Yu, Seungho and Massoud Kaviani. “Electrical, thermal, and species transport properties of liquid eutectic Ga-In and Ga-In-Sn from first principles.” *The Journal of chemical physics* 140 6 (2014): 064303.
67. Dahiya RS, Metta G, Valle M, et al. Tactile sensing—from humans to humanoids. *IEEE Trans Rob.* 2010;26(1):1–20.
68. Xi KL, Wang YC, Mei DQ, et al., A flexible tactile sensor array based on pressure conductive rubber for three-axis force and slip detection, 2015 IEEE/ASME International Conference on Advanced Intelligent Mechatronics (AIM) . 2015;476–481.
69. Wang H, Wang H, Wang Y, et al. Laser writing of janus graphene/kevlar textile for intelligent protective clothing. *ACS Nano.* 2020;14(3):3219–3226.
70. Wang C, Xia K, Zhang M, et al. An all-silk-derived dual-mode e-skin for simultaneous temperature–pressure detection. *ACS Appl Mater Interfaces.* 2017;9(45):39484–39.
71. Oh J, Yang JC, Kim JO, et al. Pressure insensitive strain sensor with facile solution-based process for tactile sensing applications. *ACS Nano.* 2018;12:7546–7553.
72. Basu J, Basu JK, Bhattacharyya TK. The evolution of graphene-based electronic devices. *Int J Smart Nano Mat.* 2010;1:201–223.
73. Wang C, Xia K, Wang H, et al. Advanced Carbon for Flexible and Wearable Electronics. *Adv Mater.* 2019;31:e1801072.
74. Zhang C, Deng H, Xie Y, et al. Stimulus responsive 3D assembly for spatially resolved bifunctional sensors. *Small.* 2019;15:e1904224.
75. Park S, Mondal K, Treadway RM 3rd, et al. Silicones for stretchable and durable soft devices: beyond sylgard-184. *ACS Appl Mat Interfaces.* 2018;10:11261–11268.
76. Shin H-S, Ryu J, Majidi C, et al. Enhanced performance of microfluidic soft pressure sensors with embedded solid microspheres. *J Micromech Microeng.* 2016;26:025011.
77. Park J, Wang S, Li M, et al. Three-dimensional nanonetworks for giant stretchability in dielectrics and conductors. *Nat Commun.* 2012;3:916–923.

- 78.** Kim M-G, Alrowais H, Pavlidis S, et al. Size-scalable and high-density liquid-metal-based soft electronic passive components and circuits using soft lithography. *Adv Funct Mater.* 2017;27:1–11.
- 79.** Ota H, Emaminejad S, Gao Y, et al. Application of 3D printing for smart objects with embedded electronic sensors and systems. *Adv Mater Technol.* 2016;1:1–8.
- 80.** Zheng Y, He ZZ, Yang J, et al. Personal electronics printing via tapping mode composite liquid metal ink delivery and adhesion mechanism. *Sci Rep.* 2014;4:1–8.
- 81.** Guo R, Wang X, Chang H, et al. Ni-gain amalgams enabled rapid and customizable fabrication of wearable and wireless healthcare electronics. *Adv Eng Mater.* 2018;20:1–9.
- 82.** Mohammed MG, Kramer R. All-printed flexible and stretchable electronics. *Adv Mater.* 2017;29:1604965–1604967.
- 83.** He Y, Wu Y, Fu J-Z, et al. Developments of 3D printing microfluidics and applications in chemistry and biology: a review. *Electroanalysis.* 2016;28:1658–1678.
- 84.** T. Takahashi, K. Takei, A.G. Gillies, R.S. Fearing, and A. Javey. Carbon nanotube active-matrix backplanes for conformal electronics and sensors. *Nano Letters*, 11(12):54085413, 2011.
- 85.** D.J. Lipomi, M. Vosgueritchian, B.C-K. Tee, S.L. Hellstrom, J.A. Lee, C.H. Fox, and Z. Bao. Skin-like pressure and strain sensors based on transparent elastic films of carbon nanotubes. *Nature Nanotechnology*, 6:788792, 2011.
- 86.** Yan, H.; Chen, Y.; Deng, Y.; Zhang, L.; Hong, X.; Lau, W.; Mei, J.; Hui, D.; Yan, H.; Liu, Y. Coaxial printing method for directly writing stretchable cable as strain sensor. *Appl. Phys. Lett.* 2016, 109.
- 87.** Amjadi, M.; Pichitpajongkit, A.; Lee, S.; Ryu, S.; Park, I. Highly stretchable and sensitive strain sensor based on silver nanowire-elastomer nanocomposite. *ACS Nano* 2014, 8, 5154–5163.
- 88.** Lu, N.; Lu, C.; Yang, S.; Rogers, J. Highly Sensitive Skin-Mountable Strain gauges Based Entirely on Elastomers. *Adv. Funct. Mater.* 2012, 22, 4044–4050.
- 89.** Bae, S.H.; Lee, Y.; Sharma, B.K.; Lee, H.J.; Kim, J.H.; Ahn, J.H. Graphene-based transparent strain sensor. *Carbon* 2013, 51, 236–242.

90. Wang, Y.; Wang, L.; Yang, T.; Li, X.; Zang, X.; Zhu, M.; Wang, K.; Wu, D.; Zhu, H. Wearable and highly sensitive graphene strain sensors for human motion monitoring. *Adv. Funct. Mater.* 2014, 24, 4666–4670.
91. Liu, C.X.; Choi, J.W. Analyzing resistance response of embedded pdms and carbon nanotubes composite under tensile strain. *Microelectron. Eng.* 2014, 117, 1–7.
92. Singh, S.; Kumar, N.; George, D.; Sen, A.K. Analytical modeling, simulations and experimental studies of a pzt actuated planar valveless pdms micropump. *Sens. Actuators A Phys.* 2015, 225, 81–94.
93. Rahimi, R.; Ochoa, M.; Yu, W.; Ziaie, B. Highly stretchable and sensitive unidirectional strain sensor via laser carbonization. *ACS Appl. Mater. Interfaces* 2015, 7, 4463–4470.
94. Yan, C.; Wang, J.; Kang, W.; Cui, M.; Wang, X.; Foo, C.Y.; Chee, K.J.; Lee, P.S. Graphene: Highly stretchable piezoresistive graphene–nanocellulose nanopaper for strain sensors (*Adv. Mater.* 13/2014). *Adv. Mater.* 2014, 26, 1950.
95. Kim, K.K.; Hong, S.; Cho, H.M.; Lee, J.; Suh, Y.D.; Ham, J.; Ko, S.H. Highly sensitive and stretchable multidimensional strain sensor with prestrained anisotropic metal nanowire percolation networks. *Nano Lett.* 2015, 15, 5240–5247.
96. Shi, G.; Zhao, Z.; Pai, J.H.; Lee, I.; Zhang, L.; Stevenson, C.; Ishara, K.; Zhang, R.; Zhu, H.; Ma, J. Highly sensitive, wearable, durable strain sensors and stretchable conductors using graphene/silicon rubber composites. *Adv. Funct. Mater.* 2016, 26, 7614–7625



## APPENDIX

MATLAB was the programming language used in this project. The following MATLAB toolboxes, libraries, and functions were used:

1. **Classification Learning Toolbox:** provides a platform for designing and implementing machine learning networks with algorithms to perform classification and regression analysis. Neural networks can be built from scratch, or one can make use of already pre-trained networks for faster deployment.
2. **Instrument Control Toolbox:** This toolbox allows us to connect MATLAB directly with peripheral devices or instruments such as analyzers, power supplies, signal generators, etc. With it, you can write data to or from MATLAB using TCP/IP, UDP, I2C, SPI, and Bluetooth serial protocols.
3. **echoudp:** This is used to start or stop a UDP echo server for enabling communication between a UDP server and a client.

The following python libraries or functions were used:

1. **Arduino Pressure Sensor Toolbox:** this is a pressure sensor toolbox that help to find the pressure sensor input/output data.It can read humidity and/or temperature data for display or transfer to other physical or cloud platforms.
2. **Arduino.GPIO:** General-Purpose Input/output is a row of pins on one side of a Arduino. The purpose of each GPIO pin can be designated by the user using software and can be used for multiple different purposes.
3. **smtplib:** is a python mailing library that includes the SMTP class that is used to connect to a mail server and to send messages.
4. **Urllib.request:** is a python module that provides a very simple interface for fetching and opening Uniform Resource Locators (URLs) using different protocols.

**Certificate Of Completion**

Envelope Id: FEDD875059F845258F2CB12DB8352C23	Status: Completed
Subject: Complete with DocuSign: EEThesis_Prosejnit_Ghosh_Final.pdf	
Source Envelope:	
Document Pages: 85	Signatures: 5
Certificate Pages: 2	Initials: 0
AutoNav: Enabled	Envelope Originator:
Envelope Stamping: Enabled	Jill Crist
Time Zone: (UTC-06:00) Central Time (US & Canada)	3900 University Blvd
	Tyler, TX 75799
	jcrist@uttyler.edu
	IP Address: 129.114.254.29

**Record Tracking**

Status: Original	Holder: Jill Crist	Location: DocuSign
4/10/2023 1:58:08 PM	jcrist@uttyler.edu	

**Signer Events**

Prabha Sundaravadivel  
 psundaravadivel@uttyler.edu  
 Assistant Professor  
 The University of Texas at Tyler  
 Security Level: Email, Account Authentication (None)

**Signature**

DocuSigned by:  
  
 101C1CC8E9EC4E2...  
 Signature Adoption: Drawn on Device  
 Using IP Address: 172.58.108.59  
 Signed using mobile

**Timestamp**

Sent: 4/10/2023 2:05:09 PM  
 Viewed: 4/10/2023 2:10:47 PM  
 Signed: 4/10/2023 2:10:56 PM

**Electronic Record and Signature Disclosure:**  
 Not Offered via DocuSign

Premananda Indic  
 PIndic@uttyler.edu  
 The University of Texas at Tyler  
 Security Level: Email, Account Authentication (None)

DocuSigned by:  
  
 0EE7E374D15143B...  
 Signature Adoption: Pre-selected Style  
 Using IP Address: 174.246.135.138  
 Signed using mobile

Sent: 4/10/2023 2:10:58 PM  
 Viewed: 4/10/2023 2:14:09 PM  
 Signed: 4/10/2023 2:14:15 PM

**Electronic Record and Signature Disclosure:**  
 Not Offered via DocuSign

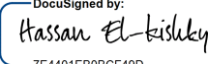
Aaditya Khanal  
 aadityakhanal@uttyler.edu  
 PI  
 The University of Texas at Tyler  
 Security Level: Email, Account Authentication (None)

DocuSigned by:  
  
 2F11EC228CD745E...  
 Signature Adoption: Pre-selected Style  
 Using IP Address: 129.114.222.13

Sent: 4/10/2023 2:14:19 PM  
 Viewed: 4/10/2023 2:17:07 PM  
 Signed: 4/10/2023 2:17:11 PM

**Electronic Record and Signature Disclosure:**  
 Not Offered via DocuSign

Hassan El-Kishky  
 helkishky@uttyler.edu  
 The University of Texas at Tyler  
 Security Level: Email, Account Authentication (None)

DocuSigned by:  
  
 7E4401EB0BCF49D...  
 Signature Adoption: Pre-selected Style  
 Using IP Address: 129.114.228.92

Sent: 4/10/2023 2:17:13 PM  
 Viewed: 4/10/2023 2:29:52 PM  
 Signed: 4/10/2023 2:30:03 PM

**Electronic Record and Signature Disclosure:**  
 Not Offered via DocuSign

Signer Events	Signature	Timestamp
Javier A. Kypuros Jkypuros@uttyler.edu Dean of the College of Engineering The University of Texas at Tyler Security Level: Email, Account Authentication (None)	 Signature Adoption: Drawn on Device Using IP Address: 104.28.48.235	Sent: 4/10/2023 2:30:06 PM Viewed: 4/10/2023 2:46:36 PM Signed: 4/10/2023 2:46:55 PM

**Electronic Record and Signature Disclosure:**  
 Not Offered via DocuSign

In Person Signer Events	Signature	Timestamp
-------------------------	-----------	-----------

Editor Delivery Events	Status	Timestamp
------------------------	--------	-----------

Agent Delivery Events	Status	Timestamp
-----------------------	--------	-----------

Intermediary Delivery Events	Status	Timestamp
------------------------------	--------	-----------

Certified Delivery Events	Status	Timestamp
---------------------------	--------	-----------

Carbon Copy Events	Status	Timestamp
--------------------	--------	-----------

Witness Events	Signature	Timestamp
----------------	-----------	-----------

Notary Events	Signature	Timestamp
---------------	-----------	-----------

Envelope Summary Events	Status	Timestamps
-------------------------	--------	------------

Envelope Sent	Hashed/Encrypted	4/10/2023 2:05:09 PM
Certified Delivered	Security Checked	4/10/2023 2:46:36 PM
Signing Complete	Security Checked	4/10/2023 2:46:55 PM
Completed	Security Checked	4/10/2023 2:46:55 PM

Payment Events	Status	Timestamps
----------------	--------	------------